Composition, Provenance, and Tectonic Setting of the Southern Kangurtag Accretionary Complex in the Eastern Tianshan, NW China: Implications for the Late Paleozoic Evolution of the North Tianshan Ocean

Zhenyu Chen, Wenjiao Xiao, Brian F. Windley, Karel Schulmann, Qigui Mao, Zhiyong Zhang, Ji'En Zhang, Chen Deng, Shuaihua Song

AGU100 ADVANCING EARTH AND SPACE SCIENCE

Tectonics

RESEARCH ARTICLE
10.1029/2018TC005385

Key Points:
- Two types of mélange are recognized in the Southern Kangurtag accretionary complex
- Composition and detrital zircon U-Pb-Hf isotopic data from sandstones indicate that they were deposited on the margin of the Central Tianshan
- Southward subduction of the North Tianshan Ocean may have lasted until the Late Carboniferous-Permian

Supporting Information:
- Supporting Information S1
- Figure S1
- Table S1
- Table S2
- Table S3
- Table S4
- Table S5

Correspondence to:
W. Xiao,
wj-xiao@mail.iggcas.ac.cn

Citation:
Chen, Z., Xiao, W., Windley, B. F., Schulmann, K., Mao, Q., Zhang, Z., et al. (2019). Composition, provenance and tectonic setting of the Southern Kangurtag accretionary complex in the Eastern Tianshan, NW China: Implications for the late Paleozoic evolution of the North Tianshan Ocean. *Tectonics*, *38*, 2779–2802. https://doi.org/10.1029/2018TC005385

Received 30 OCT 2018
Accepted 14 JUL 2019
Accepted article online 19 JUL 2019
Published online 5 AUG 2019

Composition, Provenance, and Tectonic Setting of the Southern Kangurtag Accretionary Complex in the Eastern Tianshan, NW China: Implications for the Late Paleozoic Evolution of the North Tianshan Ocean

Zhenyu Chen[1,2], Wenjiao Xiao[1,2,3], Brian F. Windley[4], Karel Schulmann[5,6], Qigui Mao[7], Zhiyong Zhang[1,2], Ji'en Zhang[1,2], Chen Deng[1,2], and Shuaihua Song[1,2]

[1]State Key Laboratory of Lithospheric Evolution, Institute of Geology and Geophysics, Chinese Academy of Sciences, Beijing, China, [2]College of Earth Sciences, University of Chinese Academy of Sciences, Beijing, China, [3]Xinjiang Research Center for Mineral Resources, Xinjiang Institute of Ecology and Geography, Chinese Academy of Sciences, Urumqi, China, [4]Department of Geology, University of Leicester, Leicester, UK, [5]IPSG, Faculty of Science, Charles University, Prague, Czech Republic, [6]Géosciences Montpellier UMR-CNRS 5243, Montpellier, France, [7]Beijing Institute of Geology for Mineral Resources, Beijing, China

Abstract The Kangurtag belt in the Eastern Tianshan, connecting the Dananhu Arc with the Central Tianshan Arc, contains diagnostic rocks of accretionary origin, and thus provides key information about the evolution of the North Tianshan Ocean. The Southern Kangurtag belt is composed of two types of mélange. Type I mélange consists of Enriched Mid-Ocean Ridge Basalt-type pillow basalts, draped by biohermal limestones and carbonate-siliceous sediments of a slope facies, and siliceous argillites from a hemipelagic-pelagic environment that together make up a seamount assemblage. In Type II mélange, Normal Mid-Ocean Ridge Basalt and ribbon cherts were dismembered and entrained in a clastic matrix, showing a "block-in-matrix" structure. Detrital zircons of four sandstones from Devonian and Carboniferous strata within the mélanges have a predominant age population of 410–430 Ma and a distinct Proterozoic cluster around 1.4–1.6 Ga. The εHf(t) values of Phanerozoic zircons range from −25.1 to +8.6. Such age patterns, typical of the Central Tianshan Arc, and the Hf isotopic data indicate that these sedimentary successions were deposited on the northern margin of the Central Tianshan Arc. The youngest detrital zircon age of 317 Ma provides an upper limit for the time of formation of the Southern Kangurtag accretionary complex. Therefore, we suggest that the Southern Kangurtag belt comprises an accretionary complex that developed during southward subduction of the North Tianshan Ocean beneath the Central Tianshan Arc. This subduction began in the Early Ordovician and may have lasted until the Late Carboniferous–Permian.

1. Introduction

The Altaids or Central Asian Orogenic Belt is the largest and longest-lived Phanerozoic accretionary orogen on Earth. Its evolution from the Neoproterozoic to early Mesozoic involved accretion of multiple continental blocks, microcontinents, seamounts, arcs, and ophiolites in the Paleo-Asian Ocean (Jahn et al., 2000, Jahn, 2004; Kröner et al., 2007; Sengör et al., 1993; Xiao et al., 2004, 2009, 2015). The Paleo-Asian Ocean has the paleogeography of an archipelago with multiple oceans and subduction zones and is similar to that of the present SW Pacific (Hsü et al., 1995; Windley et al., 2007; Xiao et al., 2003). Situated to the north of the Yili-Central Tianshan Arc, the North Tianshan Ocean (NTO) was an important branch of the southern Paleo-Asian Ocean remnants of which provide critical constraints on the accretionary history and final amalgamation of the southern Central Asian Orogenic Belt (Figure 1; Xiao et al., 2009, 2013; Zhang et al., 2015, Zhang, Zhao, Sun, et al., 2016; Zhang et al., 2018).

The timing of closure of the NTO has long been a topic of controversy with different opinions ranging from pre-Devonian collision (Charvet et al., 2007; Shu et al., 2002; Zhu et al., 2004) to Early Carboniferous collision (Li et al., 2003; Ma et al., 2014), to Late Carboniferous-Early Permian collision (Chen et al., 2011; Xiao et al., 2004; Zhang, Zhao, Sun, et al., 2016; Zhang et al., 2018). Nonetheless, most researchers have agreed

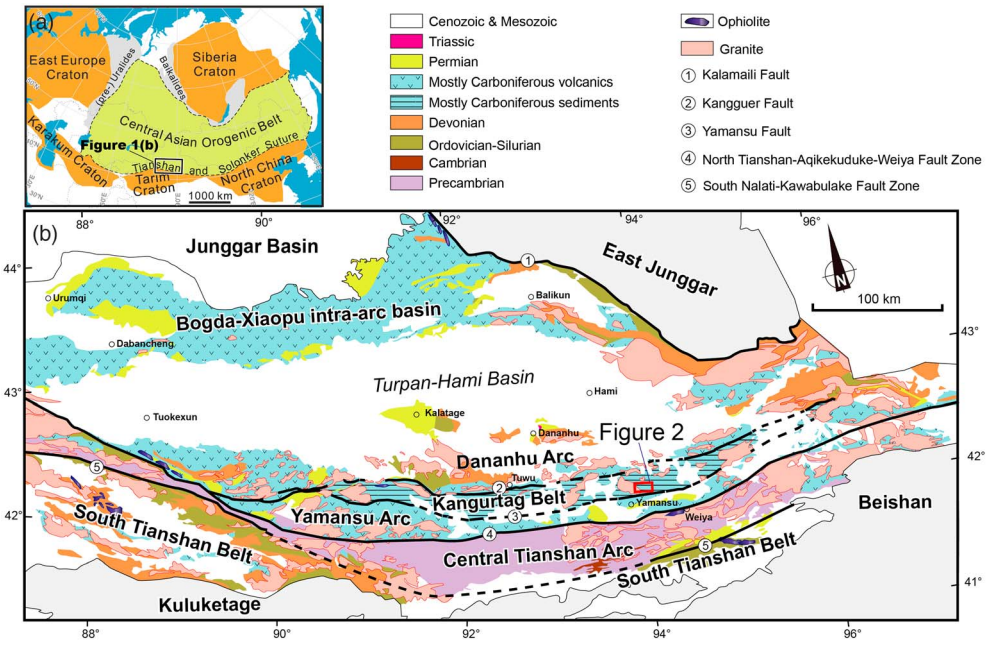

Figure 1. (a) Tectonic sketch map of the Central Asian Orogenic Belt and adjacent cratonic blocks, modified after Sengör et al. (1993) and Windley et al. (2007). (b) Simplified geological map of the Eastern Tianshan (modified after Wang, 2007). The position of Figure 2 is marked.

that the Aqikkuduk-Weiya belt (④ in Figure 1b) was the final suture associated with closure of the NTO. It records the collision between two arcs, which are a Paleozoic intra-oceanic arc in the north (North Tianshan belt) and a Paleozoic continental arc in the south (the Central Tianshan Arc; Figure 1b). This idea is supported by significant differences in the stratigraphy across the Aqikkuduk-Weiya belt together with the presence of ophiolitic rocks and a large-scale strike-slip displacement along the Aqikkuduk-Weiya belt (Chen et al., 2012; Li et al., 2003; Shu et al., 2002). However, recently, this view was challenged by the discovery of inherited Precambrian zircons in Carboniferous volcanic rocks of the Yamansu Arc (Figure 1b) suggesting that it was part of the Central Tianshan arc system, which contains Precambrian rocks (Luo et al., 2016; Zhang et al., 2018). Thus, different evolutionary models of the Yamansu Arc have led to different ideas about the boundary between the two arcs, and this has had an influence on understanding where and when the NTO closed. Therefore, in addition to the inherited zircons and arc magmatism, more evidence is required to clarify the formation of the Yamansu Arc and the polarity of subduction. Accretionary complexes are important recorders of the components of subduction (Byrne & Hibbard, 1987; Leggett et al., 1979, 1985; McKerrow et al., 1977; McCall & Kidd, 1982; Moore & Karig, 1980; Moore & Silver, 1987). Within an accretionary complex, the upper plate is the main source of terrigenous clastic sediments, as in the Makran accretionary complex (Mohammadi et al., 2016) and the Chugach accretionary complex (Amato et al., 2013). The provenance of terrigenous clastic sediments within an accretionary complex can be used to delineate the upper plate, and the positional relationship between an arc and an accretionary complex can be used to define the polarity of subduction.

In order to investigate the formation of the Yamansu Arc, we carried out field investigations along the northern side of the arc and the southern Kangurtag belt. The SE Kangurtag belt contains sparse ophiolites and mélanges (Xiao et al., 2004), which we mapped in detail (1:10,000 for Figure 2 and 1:1000 for Figure 3) in order to better define the composition of the mélange. LA-ICP-MS U-Pb and Lu-Hf isotope analyses were obtained to better understand the provenance of the terrigenous clastic rocks. This method is applicable because previous studies have demonstrated there is a significant difference in the isotopic signatures of Paleozoic magmatism between the Dananhu Arc and the Central Tianshan Arc. The Dananhu Arc is characterized by isotopically juvenile Paleozoic magmatism (Wang et al., 2018; Wang & Zhang, 2016; Xiao et al., 2017; Zhang et al., 2006), whereas the isotopic characters of the Paleozoic magmatic records from the Central Tianshan Arc are mixed (Huang et al., 2015; Liu et al., 2004; Ma et al., 2014; Zhang, Zhao, Eizenhöfer, et al.,

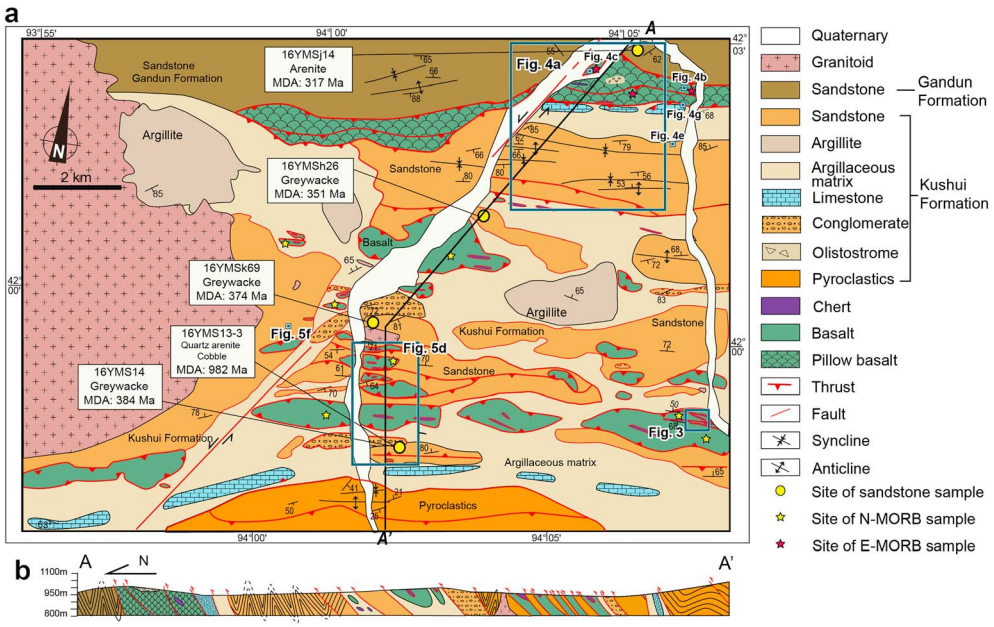

Figure 2. (a) Detailed geologic map of the Southern Kangurtag belt (see Figure 1 for location), illustrating the lithologies, spatial distribution, and structures of the mélange zone. (b) The A-A′ line of cross section shows that lithologies in the mélange zone are thrust-bounded slices. The thrusts and axial planes of folds generally dip to the south. The positions of Figures 3, 4a–4c, 4e, 4g, 5d, and 5f are marked. MDA = Maximum depositional age.

2016b). In addition, it is notable that the Central Tianshan Arc possesses a distinct zircon age cluster around 1,400–1,600 Ma, which is absent in other nearby Precambrian blocks, such as Tarim in the south, and the Tuva-Mongolia in the north (Long & Huang, 2017; Zhang, Zhao, Sun, et al., 2016). When uplifted and eroded, the clastic detritus shed from these two arc-dominated blocks would have provided different detrital zircon information.

2. Regional Background

The Eastern Tianshan, which is the easternmost segment of the Tianshan Mountain Range, occupies an important position between the Central Asian orogenic belt to the west and east (Figure 1). The Eastern Tianshan is traditionally divided into three belts from north to south: the North Tianshan belt, the Central Tianshan Arc, and the South Tianshan belt. These three belts are separated by the Aqikkuduk-Weiya fault zone and the Kawabulake fault zone, respectively (Charvet et al., 2007; Li et al., 2003; Xiao et al., 2004).

The North Tianshan belt is a composite arc comprising the Dananhu Arc in the north and the Yamansu Arc in the south. The Kangurtag belt in-between contains sparse ophiolites and accretionary complexes (Xiao et al., 2004).

The Dananhu arc (Figure 1b), located to the south of the Turpan Basin, is an intraoceanic arc characterized by isotopically juvenile Phanerozoic magmatism (460–300 Ma; Mao et al., 2018; Wang et al., 2018; Wang & Zhang, 2016; Xiao et al., 2017). The oldest strata in this belt are Ordovician volcanic and pyroclastic rocks, but Carboniferous volcanic and pyroclastic rocks are predominant. Upper Permian sediments overlie unconformably Lower Permian volcanic and pyroclastic rocks (BGMRXUAR, 1993).

To the south of the Dananhu Arc, the Kangurtag belt (Figure 1b) is an accretionary complex (Xiao et al., 2004) that is composed of major sedimentary and minor volcanic Carboniferous rocks that have been highly thrusted and imbricated (Guo & Ma, 1990; Li et al., 2003). In the north of the belt blocks of serpentinite, gabbro, dolerite, and basalt are embedded in a matrix of metasandstone (Li et al., 2005). The 494-Ma ophiolite indicates that the ocean was already in existence in the Cambrian (Li et al., 2008).

The Yamansu Arc (Figure 1b) is separated from the Central Tianshan Arc by the Aqqikkudug-Weiya ophiolitic belt to the south. This arc is composed primarily of Carboniferous volcanic and plutonic rocks

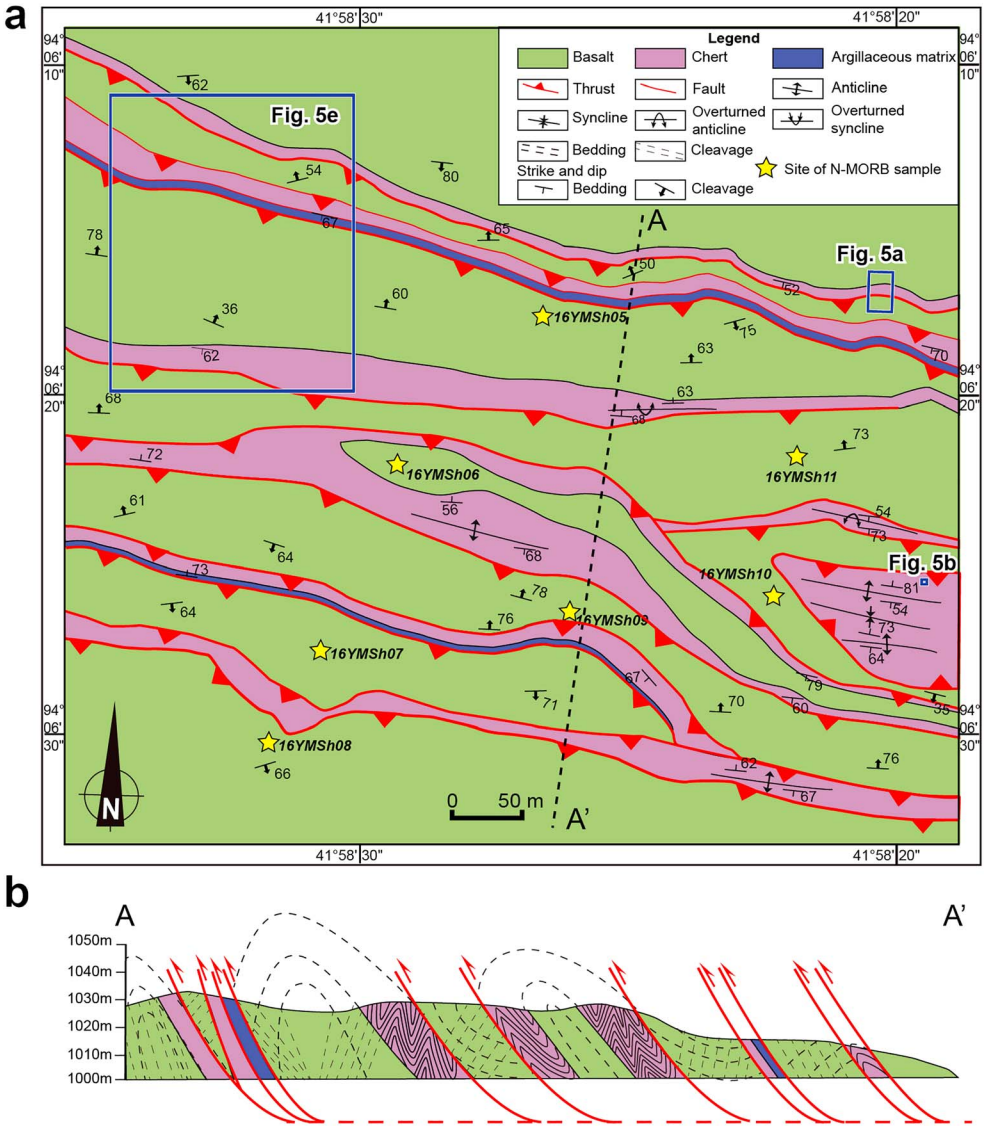

Figure 3. (a) Detailed geologic map of the basalt-chert associations. (b) The A-A′ cross section shows that the basalts and cherts are imbricated by thrusts. The positions of Figures 5a, 5b, and 5e are marked.

(Hou et al., 2006; Luo et al., 2016). The recent discovery of abundant inherited Precambrian zircons in Carboniferous volcanic rocks suggests this was a continental rather than an oceanic arc (Luo et al., 2016).

The Aqikkuduk-Weiya belt (④ in Figure 1b), located between the Yamansu Arc and the Central Tianshan Arc, consists of ophiolitic mélanges and granulites. The Weiya ophiolite mélange is composed of serpentinites, diabases, gabbros, and basalts. Late Devonian sediments unconformably overlie the ophiolitic mélange (Chen et al., 2012). The Weiya mafic granulites underwent HP metamorphism at ~538 Ma (Sm-Nd dating) and retrograde metamorphism at ~432 Ma (Ar-Ar dating) during the subduction process (Shu et al., 2004).

The Central Tianshan Arc (Figure 1b) is a continental arc built on Precambrian continental crust (Charvet et al., 2007; Liu et al., 2004). All the Precambrian gneisses, schists, migmatites, and marbles of the Xingxingxia, Kawabulake, and Tianhu Groups have undergone low- to high-grade metamorphism. Early Paleozoic magmatic rocks are extensive in the Central Tianshan Arc (Ma et al., 2014); granitic rocks are enriched in LREE relative to HREE and depleted in Nb, Ta, and Ti, which are typical signatures of subduction zone products. The arc-related magmatism may have lasted until the Late Carboniferous (Zhang, Zhao, Eizenhöfer, et al., 2016a).

3. Composition of the Southern Kangurtag Mélange

To get a better understanding of the Southern Kangurtag belt, we carried out detailed mapping (1:10,000 for Figure 2 and 1:1000 for Figure 3) to better define the composition of the mélange. As shown in Figure 2, this area is mainly composed of imbricated blocks of basalts, cherts, argillites, limestones, and greywackes in an argillaceous matrix.

Based on their different rock associations and spatial relationships, there are two types of mélange. Type I mélange mostly crops out in the north of the area (Figures 2a, 2b, and 4a). Amygdaloidal pillow basalts that are about 30 to 80 cm across in their longest dimension are predominate. The pillows are closely packed and usually have a round top and a flat or indented bottom, providing a way-up criterion (Figure 4b). Chert, clayey, or chloritic material fills the interpillow spaces (Figure 4c). In the north, pillow basalts are in fault contact with siltstones, which are interbedded with dark grey radiolarian cherts and contain clasts of basalt and limestone (Figure 4d). South of the pillow basalts biohermal crinoidal limestones are thrust onto the pillow basalts (Figure 4g), in blocks up to 30–50 m across and several kilometers long. Farther south, up to 2-km-thick turbidites have coarse-gained calcareous sandstones with graded bedding containing fragments of crinoid stems at the base (Figure 4e) and fining upward to argillites with interbedded cherts at the top (Figure 4a).

Type II mélange, only in the southern area, consists of massive basalts and abundant cherts (Figure 5a). The cherts are relatively resistant to weathering, thus often form the high-ground. Ribbon cherts contain Late Silurian—Early Carboniferous radiolarians (Li et al., 2003; Figures 5b and 5c). Both massive basalts and cherts are dismembered and thrust-imbricated with conglomerates, sandstones, and siliceous argillites (Figures 2 and 5d). Thrust-imbricated basalt-chert slices are repeated many times. Within an area of no more than 600 × 600 m (Figures 3 and 5e), there are eight repeated slices. Conglomerates contain cobble- to pebble-sized clasts of volcanic and plutonic rocks, sandstones, cherts, marbles, and shales in a sandy matrix. Conglomerates are in unconformable or faulted contact with sandstones. Locally, sandstones that are interbedded with the conglomerates (Figure 5f) are mainly feldspathic greywackes that are composed of quartz, sericitized feldspars, sedimentary lithic fragments, and minor sericites (Figure 5g).

4. Sampling

We selected 20 representative basalt samples for whole-rock geochemical analyses, as well as five terrigenous clastic rocks, including four samples of sandstones and one conglomerate for zircon U-Pb dating and Hf isotope analyses.

4.1. Basalts

There are two types of basalts: pillow bearing and massive. Amygdaloidal pillow basalts are aphyric or contain small phenocrysts of plagioclase, augite, and some olivine (Figure 6a). Massive, mostly aphyric, basalts are dismembered and irregularly distributed in a clastic matrix of greywackes and argillites. In thin section, phenocrysts in the massive basalts are mainly plagioclase, clinopyroxene, and minor magnetite in a matrix with mafic minerals, plagioclase, and Fe-Ti oxides.

4.2. Sandstones and Conglomerates

The dominant Gandun and Kushui Formations are dismembered, disordered, and imbricated with basaltic lava, spilite, keratophyre, tuff, and chert (Li et al., 2003; Xiao et al., 2004). The Late Carboniferous Gandun Formation consists of black mafic tuffaceous sandstones, siliceous argillites, and cherts. The Early Carboniferous Kushui Formation includes medium-bedded to thinly bedded greywackes, black argillites, and minor pebble/cobble conglomerates with rhythmic bedding.

We collected one sandstone sample from the Gandun Formation. Sample 16YMSj14 is a medium-grained, moderately sorted feldspathic arenite, containing subrounded to subangular quartz, feldspars, volcanic, and sedimentary lithic fragments. Four samples were collected from the Kushui Formation. Sample 16YMS14 is a fine- to medium-grained feldspathic greywacke that contains angular quartz, altered feldspars, sericites, volcanic lithic clasts, and opaque minerals. Samples 16YMSh26 and 16YMSk69 are also feldspathic greywackes but with more quartz (Figure 6b). They are medium grained and moderately sorted and are composed mainly of quartz, sericitized feldspars, together with minor sericites and sedimentary lithic fragments.

10.1029/2018TC005385

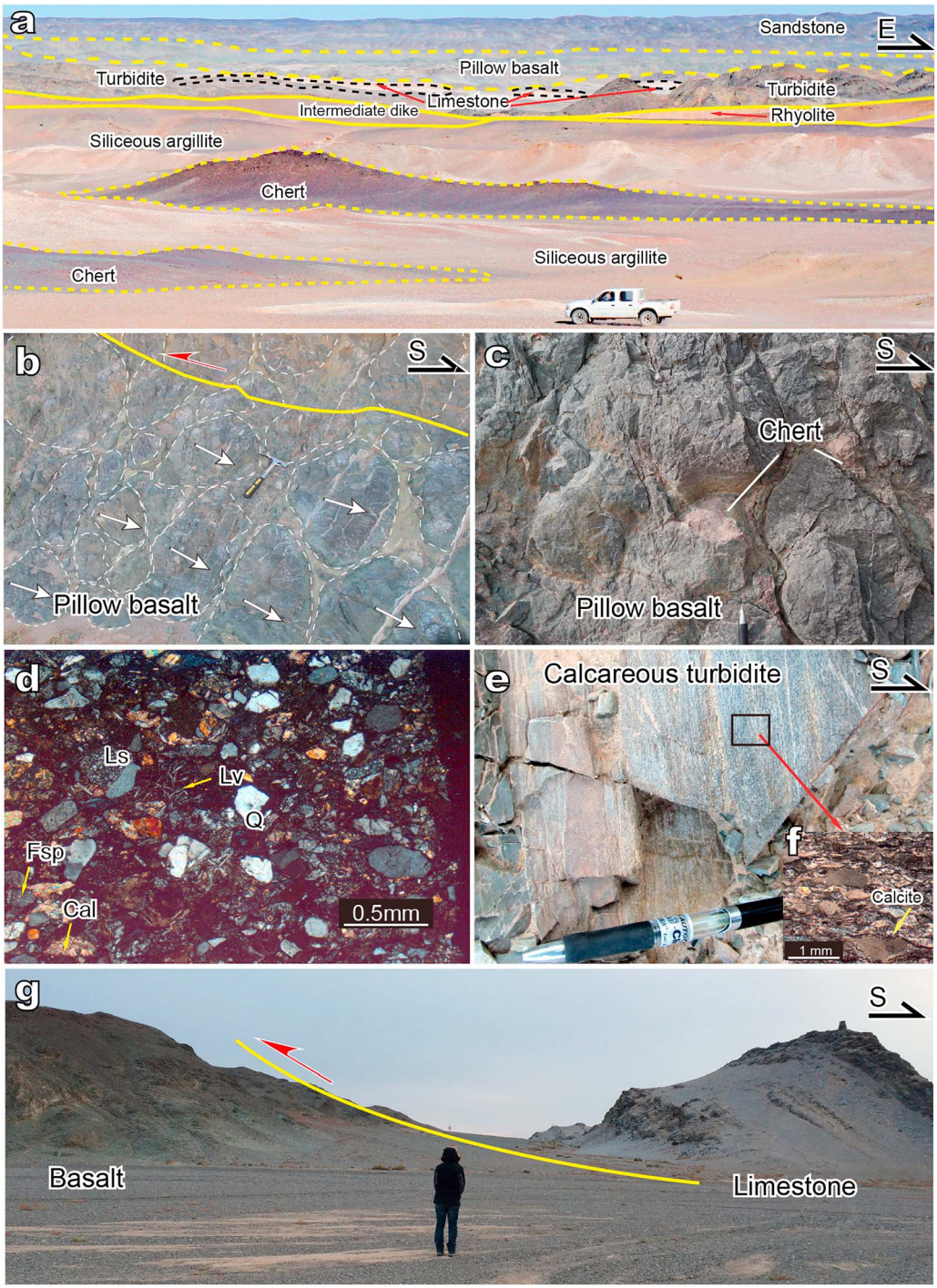

Figure 4. Photos of representative outcrops in the type-I mélange of the southern Kangurtag belt (see Figure 2 for the location). (a) Panoramic view of the type-I mélange, car for scale. (b) Thrust developed within pillow basalts (arrows point upward). The pillows have a rounded upper surface and an indented base, hammer for scale. (c) Cherts fill interpillow spaces, pen for scale. (d) Feldspathic arenite from the Gandun Formation contains fragments of basalt and limestone (calcite). (e) Field view of calcareous turbidites, pen for scale. (f) Photomicrograph of calcareous turbidite. (g) Limestones thrusted onto basalts, person for scale. Q = quartz; Fsp = feldspar; Cal = calcite; Pl = plagioclase; Lv = volcanic lithic fragment.

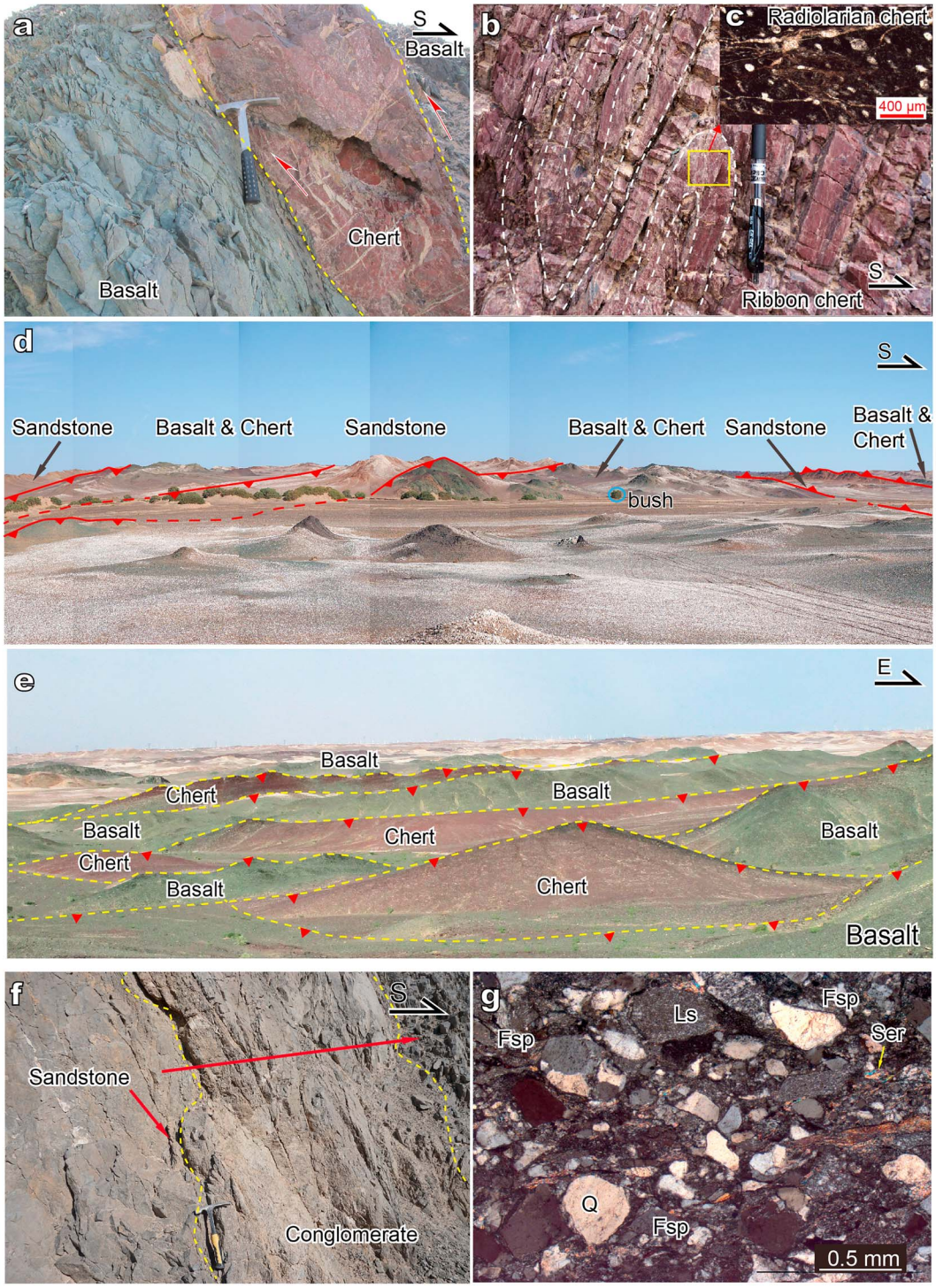

Figure 5. Representative photos of type II mélange within the Southern Kangurtag belt (see Figures 2 and 3 for the location). (a) Imbricated basalts and cherts, hammer for scale. (b) Isoclinally folded ribbon chert. (c) Photomicrograph of ribbon chert. (d) Thrusts are between imbricated sandstones, basalts, and cherts, bush for scale. (e) Basalts and cherts are repeated by layer-parallel thrusts to form duplex structures. (f) Sandstones are interbedded with conglomerates. (g) Feldspathic greywackes. Q = quartz; Fsp = feldspar; Pl = plagioclase; Ls = sedimentary lithic fragment; Ser = sericite.

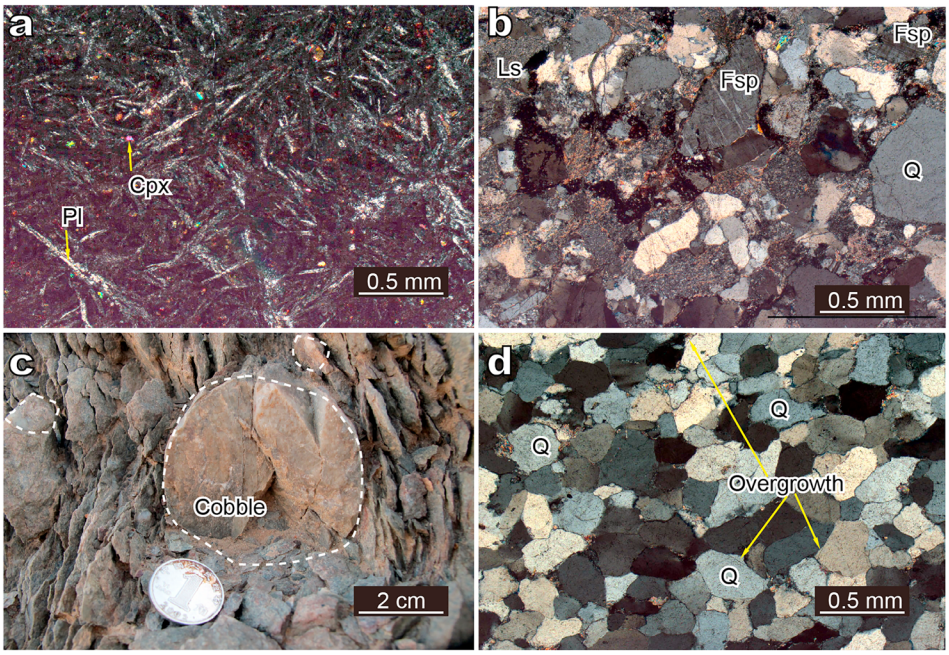

Figure 6. Photos of representative samples from the Southern Kangurtag mélange. (a) Photomicrograph of pillow basalts. (b) Photomicrograph of feldspathic greywackes from the Kushui Formation. (c and d) Outcrop and photomicrograph of a quartz arenite cobble from the Kushui Formation. Q = quartz; Fsp = feldspar; Pl = plagioclase; Ls = sedimentary lithic fragment; Cpx = clinopyroxene.

Sample 16YMS13-3 is a quartz arenite cobble collected from a conglomerate interbedded with greywacke (Figures 6c and 6d). The quartz arenite cobble consists of more than 99% quartz and has a polygonal fabric. The marked quartz at the bottom of Figure 6d is surrounded by a quartz overgrowth.

Sample locations are shown in Figure 2a. Locations, lithologies, and stratigraphic units of the samples are summarized in supporting information Text S1.

5. Analytical Methods

5.1. Whole-Rock Major and Trace Element Analyses

The analysis of major and trace elements of the bulk-rock samples was carried out at the Mineral Division of ALS Chemex (Guangzhou) Co. Ltd in Guangzhou.

Major elements were analyzed by X-ray fluorescence spectrometry (Rikagu RIX 2100). All samples were first milled to less than 200 mesh then mixed with $Li_2B_4O_7$ and $LiBO_2$ to make homogeneous glass disks at 1050–1100 °C for further analysis. The analytical precision of major elements was better than 1%.

The trace element concentrations of the sample solutions were determined by inductively coupled plasma mass spectrometry (PerkinElmer Elan 9000). About 50 mg of powder for every sample was added to a lithium metaborate flux, mixed well and fused in a furnace at 1000 °C. The resulting melt was then cooled and dissolved in 100 ml of 4% HNO_3 solution for further analysis. The analytical precision is better than 5% for most trace elements.

5.2. Zircon U-Pb Dating and Hf Isotopes

Zircon grains were separated with conventional heavy liquid and magnetic techniques, then mounted in epoxy resin and polished to about half their grain size. Cathodoluminescence (CL) images were taken using a CAMECA SX-50 microprobe at the Institute of Geology and Geophysics, Chinese Academy of Sciences in Beijing to obtain high-resolution imaging of the internal structure of the zircons. These images were used to choose potential spots for the U-Pb dating and Hf isotope analyses.

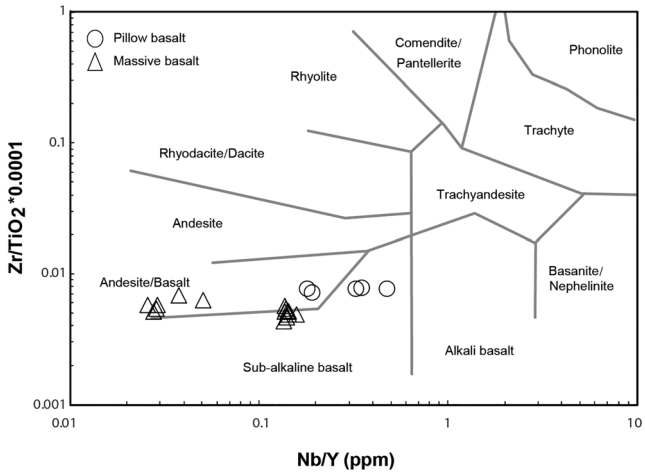

Figure 7. Geochemical Nb/Y versus Zr/(TiO_2 × 0.0001) classification diagram for the basalts from Southern Kangurtag mélange (pillow basalt and massive basalt samples are marked by circles and triangles, respectively; Winchester & Floyd, 1977).

U-Pb dating of zircons was undertaken with an Agilent 7500a quadrupole (Q)-ICP-MS with a 193-nm excimer ArF laser ablation system at the Institute of Geology and Geophysics, Chinese Academy of Sciences. The analyses were made with a beam diameter of 50 μm, 8-Hz repetition rate following analytical procedures described by Wu et al. (2010). Zircon 91500 was used as the primary standard, and NIST 610 silicate glass was used to optimize the instrument. U, Th, and Pb concentrations were calibrated with ^{29}Si as an internal standard and NIST 610 as reference material. The raw data were processed using the Glitter program (version 4; Jackson et al., 2004). For the weighted mean age calculations and concordia plots, we used the ISOPLOT program (version 3.0; Ludwig, 2003).

In situ zircon Lu-Hf isotopic analysis was carried out with a Neptune Plasma multicollector ICP-MS coupled with a 193-nm COMPexPro laser ablation system at the Institute of Geology and Geophysics, Chinese Academy of Sciences. Lu-Hf isotopic measurements were performed on or nearby the spots generated by the U-Pb analyses. The analyses were made with a beam diameter of 50 μm, 8-Hz repetition rate. The detailed analytical procedures and isobaric interference corrections were described by Wu et al. (2006). The ^{176}Lu decay constant of 1.865×10^{-11} $year^{-1}$ (Scherer et al., 2001) and the chondritic values of $^{176}Hf/^{177}Hf = 0.282772$ and $^{176}Lu/^{177}Hf = 0.0332$ (Blichert-Toft & Albarède, 1997) were adopted to calculate initial $^{176}Hf/^{177}Hf$ ratios and εHf(t) values.

6. Results

6.1. Major Elements

Major and trace element data for the basalts are presented in supporting information Table S1. The loss on ignition (LOI) for the rocks in this study ranges from 1.53 to 7.47 wt.%. All analyzed samples are basaltic in composition with silica contents ranging from 41.95 to 50.52 wt.%.

The pillow basalts in the northern area display variations in SiO_2 ranging from 41.95 to 49.15 wt.% and Al_2O_3 from 14.80 to 16.62 wt.%, in MgO from 4.37 to 8.32 wt.%. These rocks have relatively high TiO_2 contents (1.91–2.26 wt.%), total alkalis ($Na_2O + K_2O$; 3.11–5.78 wt.%), and low contents of K_2O (0.1–0.55 wt.%). The data show a subalkaline basaltic affinity on a Zr/(TiO_2 × 0.0001)–Nb/Y diagram (Figure 7).

The massive basalts from the southern area are subalkaline basalts (Figure 7) that have a concentration of K_2O (0.14 wt.% in average), Na_2O (2.49–3.81 wt.%), and high contents of TiO_2 (1.14–2.09 wt.%). The MgO contents vary from 6.60 to 8.15 wt.%.

6.2. REE and Trace Elements

Normalized to the C1 Chondrite (Sun & McDonough, 1989) the pillow basalts have moderate LREE-enriched patterns (LaN/YbN = 1.72–2.71), similar to Enriched Mid-Ocean Ridge Basalt (E-MORB; Figure 8a). In multielement variation diagrams (Figure 8b), the pillow basalts are enriched in large ion lithophile elements (LILEs), have weak depletions to enrichments in Nb, Ta, and Ti, and no obvious Eu anomalies (0.82–1.06). These features resemble those of typical E-MORB (Frey et al., 1993; Hemond et al., 2006).

The massive basalts show marked depleted LREE-enriched patterns (LaN/YbN = 0.30–1.13), similar to those of Normal Mid-Ocean Ridge Basalt (N-MORB; Figures 8c and 8e), and LREEs are more highly fractionated than HREEs. Based on their concentration of HREE, the massive basalts are divisible into two subtypes. Type I has a relatively flat HREE pattern (Figure 8c), whereas type II has a slightly depleted distribution pattern (Figure 8e). In multielement variation diagrams (Figures 8d and 8f), Type I basalts show weak depletion in Nb and Ti, and no striking Eu anomalies (0.79–1.14); Type II basalts are slightly enriched in Ta and Ti with positive Eu anomalies (0.96–1.28) and Sr anomalies. These features are comparable to those of typical N-MORB (Schilling et al., 1983; Sun et al., 1979). However, the abundance of the LILEs, Ba, U, Sr is relatively high.

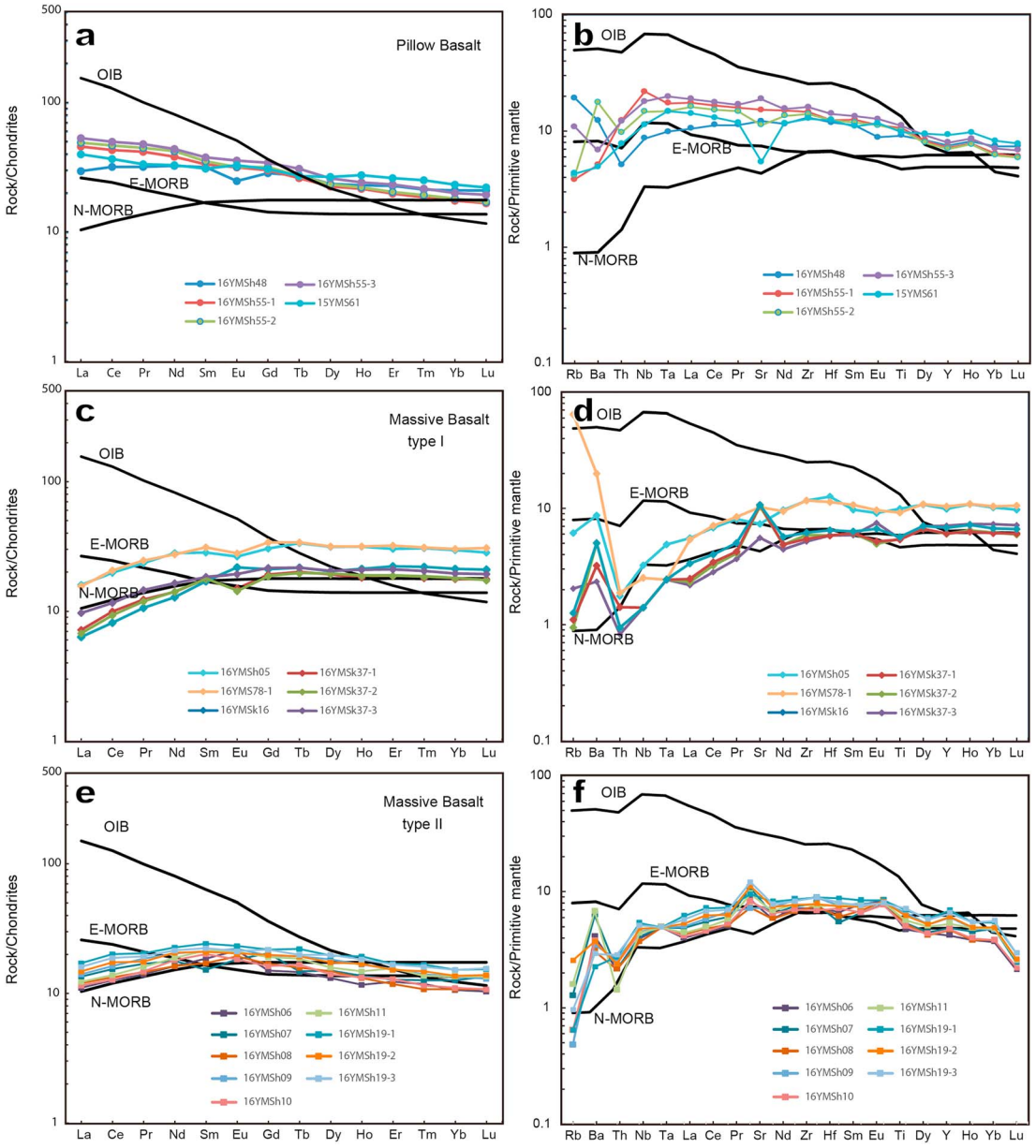

Figure 8. Chondrite-normalized REE patterns and primitive mantle (PM)-normalized multielement diagrams for basalts from the Southern Kangurtag mélange. The chondrite values are from Boynton (1984). The PM, Normal Mid-Ocean Ridge Basalt (N-MORB), Enriched Mid-Ocean Ridge Basalt (E-MORB), and OIB values are from Sun and McDonough (1989).

6.3. Analyses of Detrital Zircons for U-Pb Dating and Hf Isotopes

In this study, 400 zircons from four sandstone samples and 110 zircons from one quartz arenite cobble were selected for U-Pb analyses. After U-Pb data reduction, we carried out in situ Hf isotope analyses of all Phanerozoic detrital zircon grains except for those which were too tiny to analyze. For the sandstones, 37 of the analyses were abandoned due to their discordant ages (concordance out of 90% and 110%). The remaining 363 analyses gave U-Pb ages ranging from 315 to 3,400 Ma. Paleozoic ages account for 64% of the results. The Paleozoic grains are commonly light or rose-colored and 80–220 μm in length and have euhedral/prismatic shapes (aspect ratios 3.0–1.0). These features suggest that the Paleozoic zircons are mostly magmatic in origin, as also indicated by their typical oscillatory zoning and relatively high Th/U ratios (0.2–1.8).

In comparison, Precambrian zircons are commonly colorless to dark purple, have lengths of 70–170 μm and subrounded to well-rounded shapes. Most of the Precambrian zircons have Th/U ratios higher than 0.2 and

oscillatory zones, which are indicative of a magmatic origin. Some metamorphic zircons are also present, as suggested by their homogeneous or sector/irregular zones and their low Th/U ratios.

Zircon grains from sample 16YMSj14 of the Gandun Formation are predominantly euhedral to subhedral, have a length of 50–160 μm, and aspect ratio of 1–4. On CL images most grains show oscillatory or patchy linear zoning with Th/U ratios falling in a range of 0.18–0.92. In total, 94 concordant analyses were obtained from 100 zircon grains. As illustrated in a pie chart, the Phanerozoic zircons make up 81% of the total analyses, while the Precambrian zircons account for the remaining 19%. Zircons from this sample define one main age peak of ~427 Ma (Figure 9c), but some yielded older age clusters of ~908 and ~1,530 Ma. In total, 18 analyses yielded Precambrian ages of 563–2,937 Ma. Lu-Hf isotopic analyses of Phanerozoic detrital zircons yielded εHf(t) values ranging from −13.8 to +6.2 (Figure 10a).

Zircon grains from sample 16YMSh26, 16YMSk69, and 16YMS14 that were taken from the Kushui Formation range from colorless to brown and have lengths of 50–150 μm and aspect ratios of 1–4. Most grains have oscillatory or patchy linear zones on CL images, and their Th/U ratios are in a range of 0.09–1.05. A total of 300 zircon grains were analyzed 269 of which are concordant. As demonstrated on the pie chart, the Phanerozoic zircons make up 32%–50% of the total analyses, while the Precambrian zircons account for the remainder. Zircons from these samples define one Phanerozoic age peak of ~420 Ma (Figures 9d–9f). The Precambrian zircons yielded age clusters of~850, ~900, ~1,200, ~1,550, ~1,900, and ~2,500 Ma. The Phanerozoic zircons are characterized by a large variation of εHf(t) values (−25 to +8.6; Figures 10b–10d).

For sample 16YMS13-3, 104 concordant analyses were obtained from 110 zircon grains. Zircons from the sample are well rounded with an average length of approximately 100 μm, some of which show oscillatory zones under CL images. Th/U ratios of these zircons are in a range of 0.07–1.67. All zircons from this sample are Precambrian in age, and the major peak is at ~1,513 Ma (Figure 9g).

7. Discussion

7.1. Petrogenesis and Tectonic Setting of the Basalts

Both the pillow basalts and massive basalts had a high LOI values (LOI = 1.53–7.47 wt.%;), which probably resulted from post magmatic hydrothermal activity, which is commonly recorded by chlorites and carbonate veins (supporting information Figure S1). The alteration may have mobilized most major elements and some LILEs such as Ba, Rb, Th, Sr, U, and K as reflected in their wide variation in our rocks. However, most "immobile" elements, especially the high-field strength elements such as Nb, Ta, Zr, Hf, and Y, are resistant during alteration (Pearce & Cann, 1973; Winchester & Floyd, 1977). Thus, only the immobile incompatible trace elements and the REE are considered in the following discussion on the petrogenesis and tectonic setting of these magmatic rocks.

7.1.1. Pillow Basalts

The pillow basalts display a moderate enrichment in LREE with the incompatible trace element concentration reaching 10 times that of the primitive mantle values, and they have no obvious Nb, Ta, and Ti anomalies similar to those of E-MORB, precluding a subduction-related origin (Sun & McDonough, 1989; Figures 8a and 8b). Ratios of trace elements with different incompatibility are typically fractionated during magmatic processes and may provide important information on petrogenetic history (Weaver, 1991). As shown by immobile incompatible trace elements, like Nb, Yb, Zr, and Y, all the pillow basalt samples marked by circles plot within or near the field of E-MORB on a Hf/3–Ta–Th diagram (Wood, 1980) and on a 2Nb–Zr/4–Y triangular diagram (Meschede, 1986) (Figures 11a and 11b). Thus, we conclude that the pillow basalts were derived from a location where a spreading center encountered a mantle plume or an enriched area in the upper mantle (Fitton, 2007).

7.1.2. Massive Basalts

The massive basalts clearly show depleted LREE-enriched patterns and no anomalies in high-field strength element (e.g., Nb, Ta, Zr, and Hf), as seen in their chondrite-normalized REE and primitive mantle-normalized trace-element patterns (Figures 8c–8f). These characteristics strongly suggest that the massive basalts bear an N-MORB geochemical signature. For the Ti and Eu anomalies in type II basalts (Figure 8f), an enrichment in Ti indicates that the massive basalts contain cumulate Fe-Ti oxides. This is consistent with the occurrence of several percent ilmenite grains in thin section. Moreover, the presence of

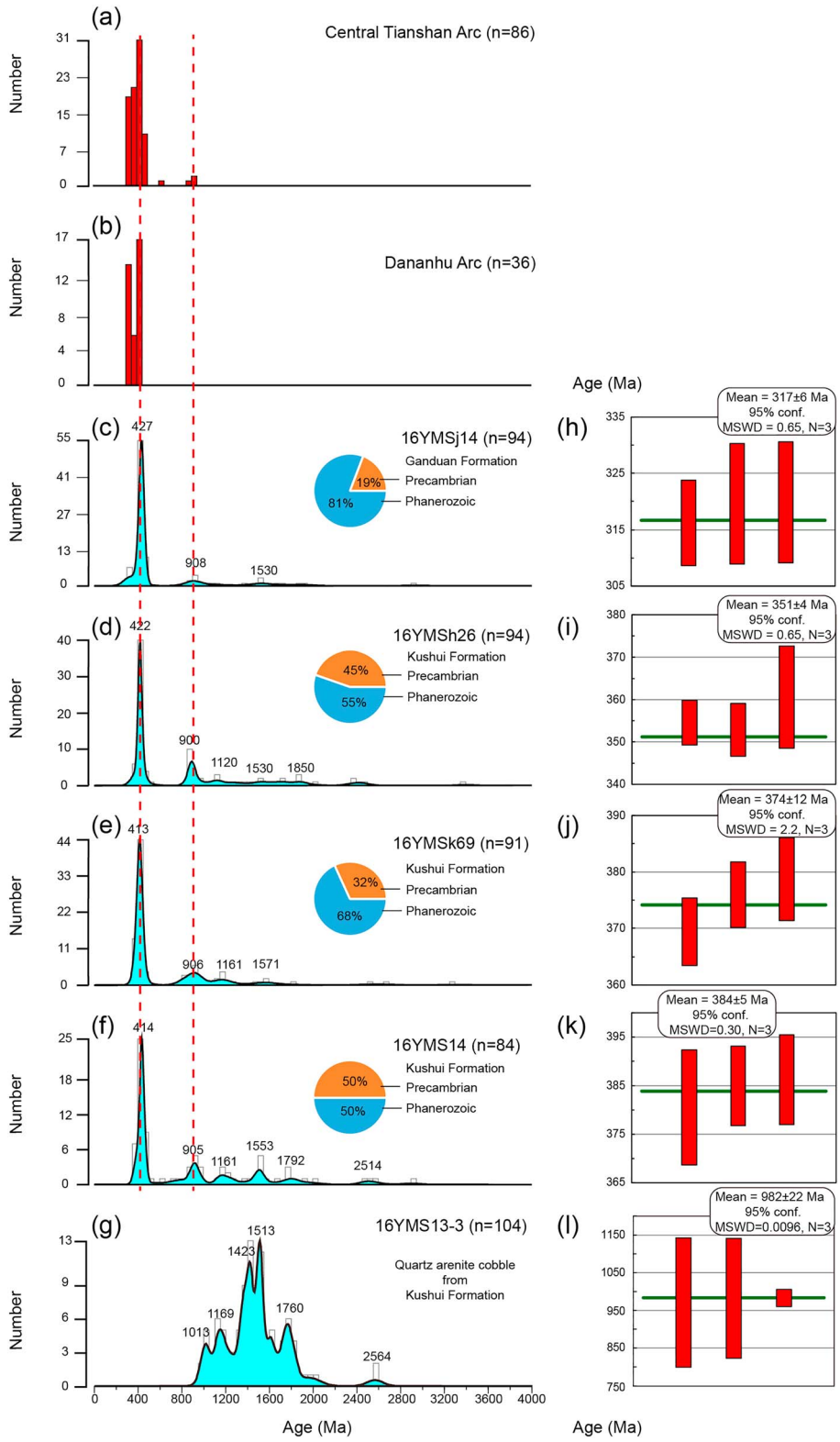

Figure 9. (a and b) Histograms for compiled crystallization ages (>300 Ma) of felsic-intermediate magmatic rocks in the Dananhu and Central Tianshan Arcs (see supporting information Table S4 for data sources). (c–g) Histograms and normalized kernel density plot curves for detrital zircon ages of five samples analyzed in this study (see Figure 2a for sample locations and supporting information Table S2 for data sources); Pie charts show the proportions of Precambrian and Phanerozoic zircons. (h–l) Maximum depositional ages (see text for details).

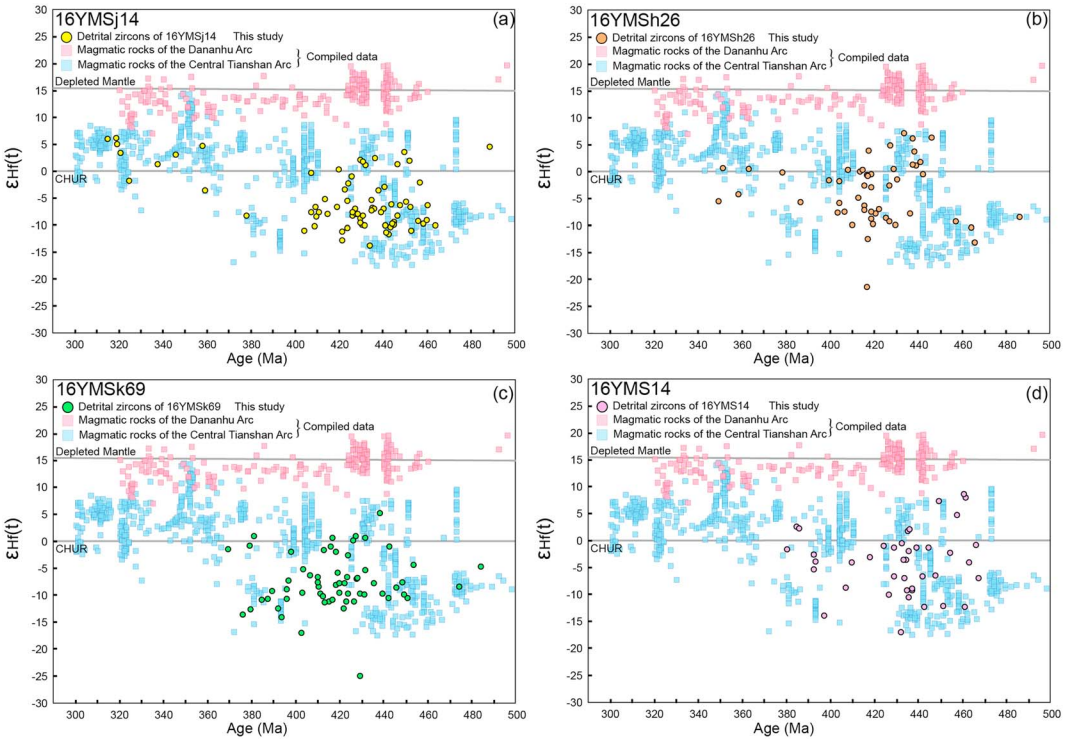

Figure 10. Plots of εHf(t) versus U-Pb ages of detrital zircons from the Southern Kangurtag mélange and magmatic zircons from the Dananhu and Central Tianshan Arcs (the Dananhu Arc (Sun et al., 2017; Wang & Zhang, 2016; Wang, Xue, Wang, et al., 2015, Wang, Xue, Liu, et al., 2015, Wang, Zhang, & Liu, 2016, Wang, Zhang, Liu, & Que, 2016; Xiao et al., 2017; Zhang, Wang, et al., 2016) and the Central Tianshan Arc (Huang et al., 2015; Lei et al., 2011, 2014; Li et al., 2016; Li et al., 2017; Ma et al., 2013, 2014; Nijat et al., 2015; Shi et al., 2014; Xu et al., 2010; Yang et al., 2012; Zhang et al., 2015; Zhang, Zhao, Eizenhöfer, et al., 2016a, 2016b; Zhu et al., 2011)). See supporting information Tables S3 and S5 for data sources.

positive Sr and Eu anomalies results from the accumulation of plagioclase. Plagioclase has a higher partition coefficient for LREEs than HREEs, while the opposite is true of clinopyroxene, and plagioclase is highly enriched in Eu over the other REEs. Thus, samples with a high plagioclase/clinopyroxene ratio have higher Eu/Eu*, higher La/Sm and a slight depletion in HREE (Perk et al., 2007). In triangular diagrams based on immobile incompatible trace elements like Nb, Yb, Zr, and Y, the massive basalt samples are marked by triangles falling within the field of N-MORB, as on a Hf/3–Ta–Th diagram (Wood, 1980) and a

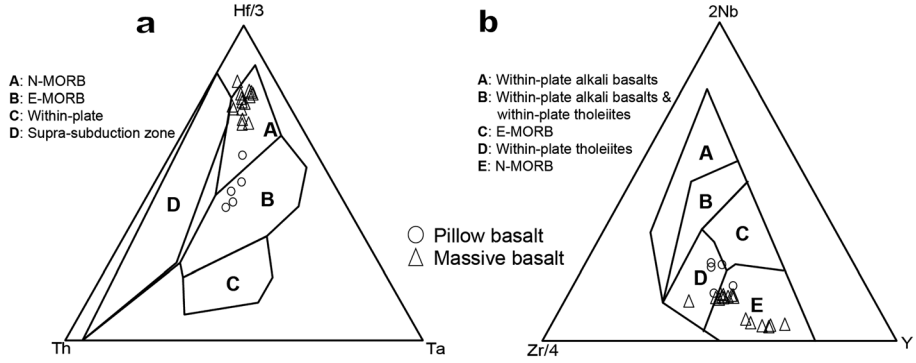

Figure 11. Triangular tectonic discrimination diagrams for basalts in the SE Kangurtag mélange (pillow basalt and massive basalt samples are marked by circles and triangles, respectively): (a) Hf/3-Ta-Th (Wood, 1980) and (b) 2Nb-Y-Zr/4 (Meschede, 1986)

2Nb–Zr/4–Y triangular diagram (Meschede, 1986; Figures 11a and 11b). Accordingly, we conclude that the massive basalts formed in a mid-oceanic ridge setting.

7.2. Maximum Depositional Ages of Strata

In this study, we apply the mean age of the youngest three or more grains, with ages overlapping at 2σ, to estimate the maximum deposition ages of the strata. Compared with the estimate of an age using only the youngest single grain, this method is more statistically reliable and more compatible with the deposition age of strata (Dickinson & Gehrels, 2009).

7.2.1. Gandun Formation

The maximum deposition age of sample 16YMSj14 is estimated at ca. 317 Ma (Figure 9h); this is in accordance with the stratigraphic position of the Gandun Formation (Late Carboniferous).

7.2.2. Kushui Formation

The stratigraphic subdivisions of the Kushui Formation have long been an issue of debate because of the lack of fossils (Ma et al., 1993). According to the biological assemblage of conodonts, Guo and Ma (1990) gave the Kushui Formation an Early Carboniferous age. However, later researchers pointed out that some of the conodont assemblages are Late Devonian in age (Ma et al., 1993). The maximum depositional ages of three samples (16YMSh26, 16YMSk69, and 16YMS14) collected from the Kushui Formation are circa 351, 374, and, 384 Ma, respectively (Figures 9i–9k). To get a confident estimate of the time of deposition from detrital zircons, there are two indispensable requirements: (1) a supply of contemporary igneous components during deposition and (2) more than 60 analysis spots (Dickinson & Gehrels, 2009; Gehrels et al., 2011). Certainly, in our case both requirements are well satisfied. In the Dananhu and Central Tianshan arcs, magmatism was active from the Late Ordorvician to Permian (Du et al., 2018; Huang et al., 2015; Huang, 2014; Ma et al., 2014; Mao, Xiao, et al., 2014; Shi et al., 2014; Wang et al., 2018; Wang & Zhang, 2016; Zhang, Zhao, Eizenhöfer, et al., 2016a; Zhou et al., 2010). Hence, 100 analysis points for each sample are adequate to provide robust information about their age and stratigraphic position.

From the above, we conclude that the Kushui Formation is a diachronous stratigraphic unit. The depositional process may have begun in the Devonian and lasted until the Early Carboniferous. Moreover, the maximum depositional ages of the three samples, combined with sample 16YMSj14, are 384 ± 5, 374 ± 12, 351 ± 4, and 317 ± 6 Ma, indicate a general younging toward the north.

7.2.3. Quartz Arenite Cobble of the Kushui Formation

The maximum depositional age of the quartz arenite cobble is 982 Ma (Figure 9l). Thus, the stratigraphic unit to which these quartz arenites belong may have been deposited during the Mesoproterozoic or later.

7.3. Provenance Study in the Southern Kangurtag Mélange

The 410- to 430-Ma age peak is the most predominant characteristic in the histograms of all samples (Figures 9c–9f). Detrital zircon ages within the interval of 310–460 Ma overlap with the ages of widespread Late Ordovician to Carboniferous granitic plutons of the Central Tianshan Arc (Figure 9a; Ma et al., 2014; Yin et al., 2017; Zhang, Zhao, Eizenhöfer, et al., 2016a), and the coeval magmatic activity of the Dananhu Arc may also have provided a potential source area (Figure 9b; Du et al., 2018; Wang et al., 2018; Wang & Zhang, 2016; Wang, Xue, Wang, et al., 2015, Wang, Xue, Liu, et al., 2015; Zhou et al., 2010). In this situation, detrital zircon ages alone cannot distinguish between a supply source in the Dananhu Arc and a supply sourced from the Central Tianshan Arc. Nonetheless, the Dananhu Arc is an intraoceanic arc (Mao et al., 2018; Wang et al., 2018; Wang & Zhang, 2016; Xiao et al., 2017), while the Central Tianshan Arc is a continental arc (Huang et al., 2015; Liu et al., 2004; Ma, Shu, Santosh, et al., 2012, Ma, Shu, Jahn, et al., 2012, 2014; Zhang, Zhao, Eizenhöfer, et al., 2016a). The igneous rocks of the Dananhu Arc were sourced from juvenile material that could not have been contaminated by easily fusible felsic crust of a magma from an active continental margin (Leat & Larter, 2003; Stern, 2010; Wilson, 2007). Such juvenile magmatism could intuitively be demonstrated by its isotopic character, that is, a relatively high εHf(t) value close to the curve of depleted mantle. In contrast, the Central Tianshan Arc was built on preexisting thick and felsic continental crust. Hence, the resulting magmatism was more mature than that of the Dananhu Arc. Magmatism of active continental margins can be sourced from melted ancient crust and from juvenile material. Considering Hf isotopes, active margin-related magmatism typically shows both positive and negative εHf(t) values (DeCelles et al., 2009; Mišković & Schaltegger, 2009). Therefore, in situ zircon Hf isotopes provide us with another opportunity to discriminate zircons

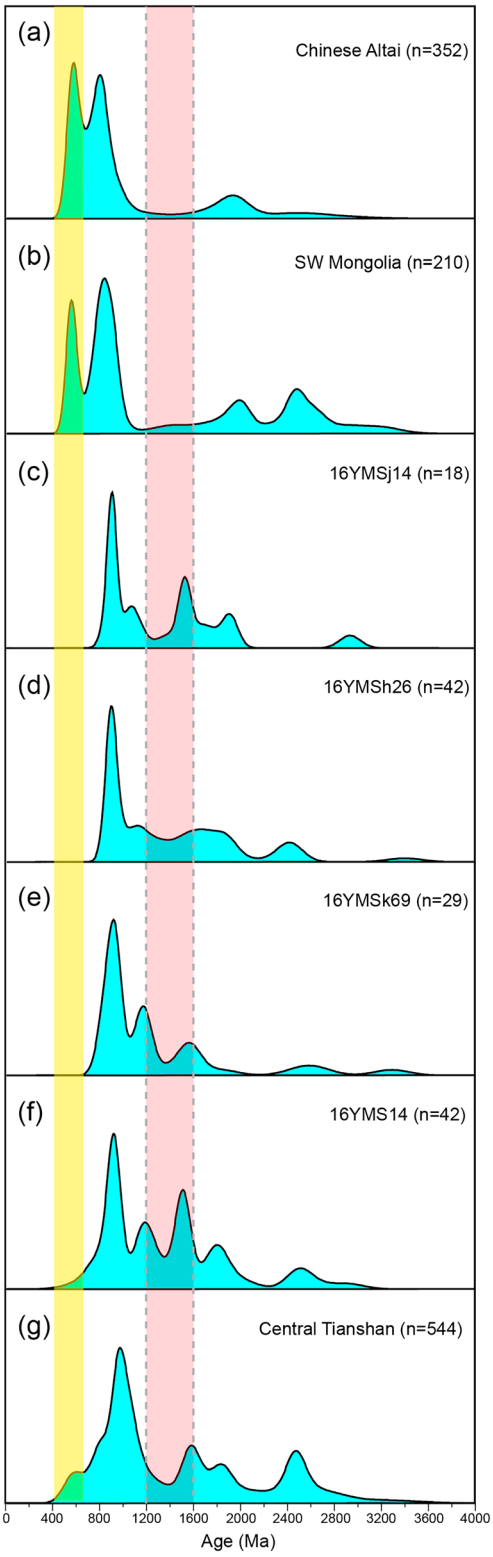

Figure 12. Normalized kernel density plot curves for detrital zircon ages of samples analyzed in this study and those of Paleozoic sandstones from the Chinese Altai (Jiang et al., 2011; Long et al., 2007; Long et al., 2010; Wang et al., 2014), SW Mongolia (Gibson et al., 2013; Jiang et al., 2012; Rojas-Agramonte et al., 2011), and the Central Tianshan Arc (see text for details). Only Precambrian ages are plotted.

from these contemporaneous magmatic environments (Figure 10; the Dananhu Arc (Sun et al., 2017; Wang & Zhang, 2016; Wang, Xue, Wang, et al., 2015, Wang, Xue, Liu, et al., 2015, Wang, Zhang, & Liu, 2016, Wang, Zhang, Liu, & Que, 2016; Xiao et al., 2017; Zhang, Wang, & Liu, 2016) and the Central Tianshan Arc (Huang et al., 2015; Lei et al., 2011, 2014; Li et al., 2016; Li et al., 2017; Ma et al., 2013, 2014; Nijat et al., 2015; Shi et al., 2014; Xu et al., 2010; Yang et al., 2012; Zhang et al., 2015, Zhang, Zhao, Eizenhöfer, et al., 2016a, 2016ab; Zhu et al., 2011)). The εHf(t) values for the Dananhu Arc are mostly >11, whereas the εHf(t) values for the Central Tianshan Arc are generally <11, and they have both positive and negative values. From relationships in the age-εHf(t) diagram, we propose that the in situ Hf isotopic character of zircons in the sandstones in this study is compatible with a source in the Central Tianshan Arc but not from the Dananhu Arc (Figures 10a–10d). Notably, even the Late Carboniferous sample (16YMSj14) contains no Dananhu Arc-like zircons with high εHf(t) (Figure 10a). Therefore, the Central Tianshan Arc was most likely the primary provenance of the sandstones in the Southern Kangurtag belt. Accordingly, until 317 Ma (the maximum depositional age of sample 16YMSj14), the sedimentary successions in the Southern Kangurtag belt were dominantly sourced from the Central Tianshan Arc, either from magmatic rocks or from recycled arc-related sediments.

Moreover, the Precambrian zircons provide additional information about possible source areas. In this study, Precambrian ages make up a majority of the total of the analyzed samples. Four samples have similar age clusters around 850–920, 1,000–1,200, 1,400–1,600, 1,800–1,900, and 2,400–2,600 Ma, which are coincident with the ages of detrital zircons from the Central Tianshan Arc (Figure 12; Ma, Shu, Santosh, et al., 2012, Ma, Shu, Jahn, et al., 2012). Precambrian zircons are generally absent in the Dananhu Arc (Mao et al., 2018; Xiao et al., 2013; Zhang et al., 2018). Nevertheless, it is noteworthy that Precambrian basements are also reported in arcs north of the Dananhu Arc, that is, the Tuva-Mongolia Arc and in the surrounding blocks, including the Chinese Altai and SW Mongolia (Kröner et al., 2010). However, there are noticeable differences in the Precambrian record of the Central Tianshan Arc and the Chinese Altai and SW Mongolia. In this study, sandstone samples from the Southern Kangurtag belt lack the conspicuous age peak of 570 Ma of the Chinese Altai and SW Mongolia, but they do have abundant age clusters ranging from 1,200 to 1,600 Ma, which is absent in both the Chinese Altai and SW Mongolia, but is prominent in the Central Tianshan Arc (Figure 12). Therefore, it is unlikely that these two blocks supplied much clastic material to the Southern Kangurtag belt.

In addition, the quartz arenite cobble (16YMS13-3) from the conglomerate interbedded with greywackes gives us one more hint of provenance. The quartz arenite boulders consist of more than 99% quartz. The maximum deposition age of this quartzite boulder is 982 Ma. Age clusters are mainly within the range of 1,200–1,600 Ma with a conspicuous age peak at 1,513 Ma (Figure 13). Quartz arenites with very similar petrography and detrital zircon age distribution occur within the Kawabulake Group of the Central Tianshan Arc (Huang, 2017). The quartz arenite of the Kawabulake Group is composed of 99% quartz, with a depositional age estimated by the youngest zircons to be 936 Ma. Thus, the approximate depositional age and high similarity in age distribution and petrography

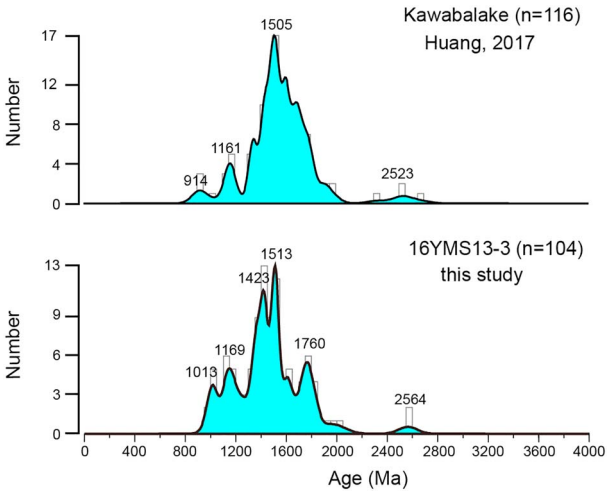

Figure 13. Normalized kernel density plot curves for detrital zircon ages in the quartz arenite cobble in this study and a sandstone from the Kawabulake Group of the Central Tianshan Arc (Huang, 2017).

suggest that the quartz arenite cobble in the Southern Kangurtag belt was likely transported from the Central Tianshan Arc and redeposited in the Southern Kangurtag belt.

Given the above evidence, we conclude that the Central Tianshan Arc in the south was the main provenance for sandstones of the Southern Kangurtag belt.

7.4. Accretionary Complex in the Southern Kangurtag Belt

It is well known that mélanges can form in a variety of tectonic settings by fragmentation and mixing processes, and the different modes of origin of mélanges lead to different compositions and structures (Festa et al., 2010; Onishi & Kimura, 1995; Wakabayashi & Dilek, 2011; Wakita et al., 2012, 2015). By large scale mapping, geochemical and provenance analysis, we obtained a detailed description of the composition and structure of the Southern Kangurtag mélange, which will contribute to an improved understanding of its tectonic setting. The lithologies and structures of the Southern Kangurtag mélange are comparable to those of fore-arc accretionary complexes in Japan, the western Pacific, and Southern Europe. In these areas, accreted oceanic materials make up the main body of accretionary complexes (Danelian & Robertson, 2001; Leggett, 1979, 1985; Isozaki et al., 1990, 2010; Kusky & Bradley, 1999; Kusky et al., 2013; Maruyama et al., 2010; McKerrow, 1977; Moore & Karig, 1980; Safonova et al., 2016; Sawaki et al., 2010; Wakita & Metcalfe, 2005).

In type I mélange of the Southern Kangurtag belt, the rock association is similar to that of seamounts (Safonova et al., 2016; White, 2010). Overall, these sedimentary successions represent sediments on the top, slope, and foot of a topographic high on the seafloor. The occurrence of crinoid stems within our biohermal limestone suggests a shallow water environment; the calcareous turbidites were likely deposited on an unstable slope; argillite and chert indicate hemiplegic-pelagic deposition. In addition, basalts with an E-MORB geochemical affinity tend to occur on seamounts that originated from a hotspot or a plume-ridge interaction, as in the Emperor Seamounts, Southern Mid-Atlantic, and Southwest and Central Indian ridges (Douglass et al., 1999; Fitton, 2007; Le Roux et al., 2002; Murton et al., 2005; Regelous et al., 2003). Thus, we suggest that type I mélange was derived from a subducted seamount.

In contrast, the type II mélange, which is composed of N-MORB-type basalts, radiolarian cherts, and siliceous mudstones in a matrix of argillites, resembles typical accreted ocean plate stratigraphy (Isozaki et al., 1990; Matsuda & Isozaki, 1991). It records the birth of an ocean with N-MORB-type basalts at a mid-oceanic ridge, the lateral movement of the ocean as it is overlain progressively by deep-sea cherts and pelagic argillites as the ocean opens, and then begins to close. Finally, it arrives at a trench, when the oceanic sediments are scraped off and mixed with trench-fill turbiditic siltstones, sandstones, and conglomerates. Frequent tectonic repetition of the chert-basalt pairs is caused by thrusting associated with the formation of duplexes during the underplating of ocean plate stratigraphy to the overriding plate (Hashimoto & Kimura, 1999; Isozaki et al., 1990; Kimura & Ludden, 1995; Matsuda & Isozaki, 1991; Wakita & Metcalfe, 2005).

Within the Southern Kangurtag mélange, the sandstones and conglomerates are disrupted and imbricated with accreted oceanic materials by south dipping thrusts. These sediments received detritus from both continental and oceanic sources. Provenance of this nature together with structure of the sandstones and conglomerates suggests that they were deposited on a trench slope. The clasts of volcanic rocks, granites, and quartz arenites were derived from an active continental margin; the fragments of basalts, cherts, and limestones came from accreted oceanic materials. Submarine canyon and smaller slope gullies serve as active conduits to bypass upslope obstruction and transport terrigenous clasts to a trench slope. Erosion of tectonic ridges formed by thrusting and folding of accreted material also provide detritus for a trench-slope (Bassett & Orlowski, 2004; Moore et al., 1980; Underwood & Bachman, 1986). On an accretionary subduction margin, thrusting and folding cause considerable disruption of the trench slope material (Underwood & Moore, 1998). In addition, sediments with such features may also originate from a fore-arc basin and be involved in the accretionary processes. In a convergent margin, contraction may result in the inversion of

a fore-arc basin, pushing the accretionary wedge backward into the fore-arc basin and forming thrusts that incorporate forearc basin sediments into the wedge (Westbrook et al., 1988).

Above all, the mélanges in the Southern Kangurtag belt have the character of an accretionary complex; the basalts and cherts were accreted by underplating.

7.5. Tectonic Nature of the Kangurtag Belt

The Kangurtag belt was envisaged as an accretionary complex that formed during northward subduction of the North Tianshan Ocean, based on the migration of magmatic fronts with time (Han & Zhao, 2018; Li et al., 2006; Mao et al., 2018; Xiao et al., 2004). In the Dananhu Arc, the magmatic front migrated from Ordovician-Silurian in the Kalatage area in the north, through Devonian in the Dananhu area, to Carboniferous in the Tuwu area in the south (Li et al., 2006).

However, our study indicates that the SE Kangurtag belt is related to southward subduction. First, the provenance of turbiditic sandstones and quartz arenites cobbles within the Southern Kangurtag mélange all point to southward subduction. The Central Tianshan source of the turbiditic sandstones and quartz arenites cobbles of the Southern Kangurtag belt agree well with an accretionary prism and arc scenario in which the supply of clastic sediments in the accretionary complex mainly came from the arc side of a subduction system (Dickinson & Seely, 1979; Ingersoll, 1988). In addition, the northward younging of the maximum age of deposition of our turbiditic sandstones also implies a northward growing accretionary prism (Figure 2a). This implies northward growth of an accretionary complex that developed during southward subduction, as well known in the Aleutians, Alaska, and Japan (Isozaki et al., 1990, 2010; Kusky & Bradley, 1999; Leggett, 1979; Maruyama et al., 2010; McKerrow, 1977; Moore & Karig, 1980). Generally, accretionary prisms grow oceanward with sediments in the accretionary prism younging oceanward, which results from roll-back of the subducting oceanic plate (Cawood et al., 2009; Taira, 2001; Taira et al., 1982). Thus, we conclude that the Southern Kangurtag belt is an accretionary prism that developed during southward subduction of the North Tianshan Ocean plate beneath the Central Tianshan Arc.

Moreover, in the NW Kangurtag belt, blocks of serpentinite, gabbro, dolerite, and basalt are thrust imbricated with a matrix of metapyroclastic rocks and andesites. The gabbros, dolerites, and basalts show suprasubduction zone, geochemical similarity. The metapyroclastic rocks and andesites belong to early Carboniferous strata of the Dananhu Arc. In combination with thrusts of a dominantly southward vergence, the NW Kangurtag mélange was suggested by Li et al. (2005) to have formed in the fore-arc of the Dananhu Arc. In conclusion, the Kangurtag belt probably contains accretionary complexes that formed by divergent double subduction. The youngest zircons that we obtained from turbiditic sandstones indicate that the subduction process lasted until 317 Ma.

7.6. Tectonic Affinity of the Yamansu Arc

The tectonic affinity of the Yamansu Arc is under debate. There are two main viewpoints: (1) The Yamansu Arc was built on the fore-arc accretionary prism of the Dananhu Arc due to rollback of the North Tianshan Ocean; this is based on southward younging of the magmatism (Han & Zhao, 2018; Xiao et al., 2004, 2013), and (2) the Yamansu Arc formed by southward subduction beneath the Central Tianshan Arc, which was initiated in the Carboniferous. This idea is supported by Central Tianshan-like inherited zircons in Carboniferous volcanic rocks from the Yamansu Arc (Luo et al., 2016; Zhang et al., 2018).

In this paper, we reconsider the tectonic affinity of the Yamansu Arc from the viewpoint of the basic structural evolution of a subduction system. In an integrated, holistic accreting-subducting system, the travel history from an ocean to a trench and arc is preserved in the stratigraphy of the trench-accretionary prism-arc complex. As discussed above, the Southern Kangurtag belt is the accretionary prism of the Central Tianshan Arc, and the Yamansu Arc is located between the Central Tianshan Arc and the Southern Kangurtag accretionary prism. From that structural environment, we conclude that the Yamansu Arc was a continental arc built on the margin of the Central Tianshan Arc. This is further supported by the coeval calc-alkaline magmatism and similar Precambrian imprint in both the Yamansu and Central Tianshan Arcs. The Carboniferous igneous rocks crop out across the Aqikkuduk-Weiya fault zone between the Yamansu Arc and the Central Tianshan Arc. The basaltic andesites and rhyolites of the Central Tianshan Arc have an island arc geochemical signature, which is no different from that of the Yamansu Arc (Mao, Wang, et al., 2014). In addition, the volcanic rocks of the Yamansu Arc contain many Precambrian inherited zircons;

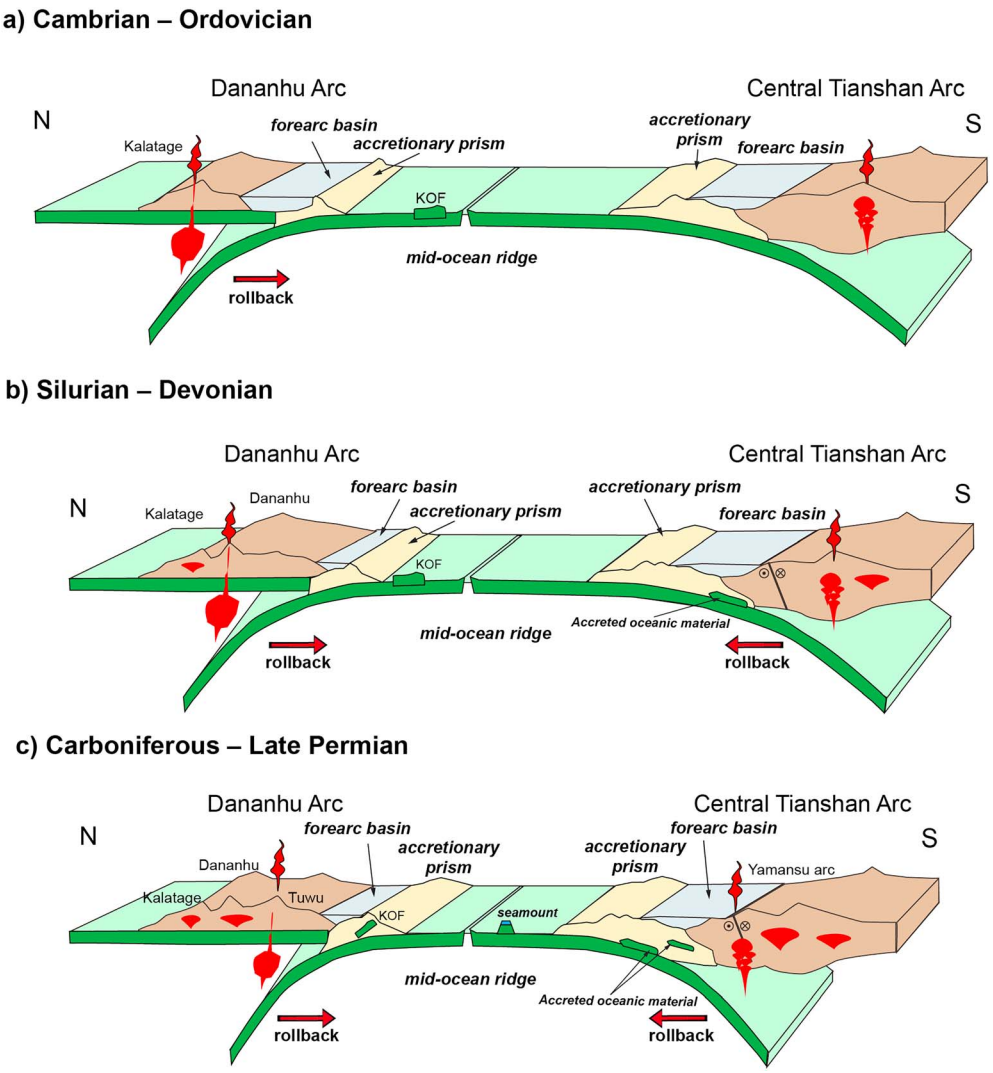

Figure 14. Schematic diagrams illustrating the tectonic evolution of the North Tianshan Ocean and adjacent areas. (a) Cambrian–Ordovician subduction of the North Tianshan Ocean generated the Dananhu Arc in the north and built the Central Tianshan Arc above a Precambrian basement in the south; (b) During the Silurian-Late Devonian, the North Tianshan Ocean continued its two-way subduction; (c) During the latest Carboniferous-Permian, southward subduction and rollback of the North Tianshan Ocean gave rise to the magmatism in the Yamansu Arc. The North Tianshan Ocean terminated along the Kangurtag belt. KOF = Kangurtag ophiolite fragments (see text for details).

the Precambrian ages cluster at ~600, ~1,000, ~1,400, ~2,200, and ~2,600 Ma, which are similar to the zircon age peaks recorded by the sedimentary and magmatic rocks of the Central Tianshan Arc (Luo et al., 2016). Finally, a 921-Ma Precambrian granite is in the western part of the Yamansu Arc (Su et al., 2008). In contrast, the Dananhu Arc has no record of Precambrian zircons or events (Mao et al., 2018; Xiao et al., 2013; Zhang et al., 2018). The 481-Ma arc-related granodiorite in the Central Tianshan Arc, the pre-Devonian Weiya ophiolite, and the Early Paleozoic top-to-north ductile-shear deformation along the Aqikkuduk-Weiya fault zone further suggest that southward subduction began as early as the Early Ordovician (Chen et al., 2012; Li et al., 2009; Tang et al., 2011).

7.7. Implications for the Tectonic Evolution of the North Tianshan Ocean

By combining and integrating our results with previously published data of the Dananhu Arc, the Yamansu Arc, the Central Tianshan Arc, and the Kangurtag belt (Xiao et al., 2004; Zhang et al., 2018), we suggest the following evolution of the North Tianshan Ocean, which involved two-way subduction with oceanward accretion in both the Dananhu Arc and the Central Tianshan Arc (Figure 14).

Stage 1 (Cambrian-Ordovician; Figure 14a)

The 494-Ma Kangurtag ophiolite suggests that the North Tianshan Ocean was already in existence in the Late Cambrian (Li et al., 2008). Later, during the Ordovician, subduction of the North Tianshan Ocean generated the Dananhu Arc in the north (Du et al., 2018) and built the Central Tianshan Arc above a Precambrian basement in the south (Ma et al., 2013).

Stage 2 (Silurian-Late Devonian; Figure 14b)

During the Silurian-Late Devonian, the North Tianshan Ocean continued its two-way subduction. In the north the magmatic front moved southward toward the Dananhu area, generating a magmatic arc in the Devonian.

Stage 3 (Carboniferous-Late Permian; Figure 14c)

The 324.8-Ma ophiolitic rocks in the North Tianshan belt indicate that the North Tianshan Ocean still existed in the Late Carboniferous (Xu et al., 2006). Also, the southward subduction of the North Tianshan Ocean beneath the Central Tianshan Arc probably continued to 317 Ma, as suggested by the youngest detrital zircons in turbiditic sandstones in the Southern Kangurtag belt.

During the Carboniferous-Late Permian, continuous subduction was accompanied by rollback. In the north, the magmatic front moved southward to the Tuwu area generating a Carboniferous magmatic arc. Permian magmatic rocks were derived from a depleted mantle source, which is similar to that of pre-Permian magmatic rocks in the Eastern Tianshan (Mao, Xiao, et al., 2014; Wang et al., 2018). Meanwhile, in the south, the northward movement of the magmatic axis created the Carboniferous magmatic belt in the Yamansu area.

Consequently, the North Tianshan Ocean was consumed during two-way subduction that created a suture between the accretionary prisms of the Central Tianshan and Dananhu Arcs. The Kangurtag belt recorded the final closure of the North Tianshan Ocean.

8. Conclusions

Our new data and interpretations lead to the following conclusions:

1. The Southern Kangurtag belt contains two types of mélange that record the subduction of seamounts and oceanic crust. Type I mélange consists of E-MORB-type pillow basalts, draped by biohermal limestones, carbonate-siliceous sediments of slope facies, and pelagic siliceous argillites. Within Type II mélange, N-MORB and ribbon cherts were dismembered and embedded in a clastic matrix.
2. The provenance of the Devonian-Carboniferous sandstones and quartz arenite cobble sampled within the Southern Kangurtag belt was the Central Tianshan Arc in the south, when any detrital supply from the Dananhu Arc or further north was out of reach.
3. The northward younging trend of the maximum deposition ages together with the spatial relationship of the interconnected accretionary complex (the Southern Kangurtag accretionary complex) and arc (the Central Tianshan Arc) indicate southward subduction of the North Tianshan Ocean beneath the Central Tianshan Arc.
4. The youngest detrital zircon age, 317 Ma, provides an upper time limit for growth of the Kangurtag accretionary complex, suggesting that subduction of the North Tianshan Ocean lasted until the Late Carboniferous-Permian.
5. In combination with previous studies, we propose a divergent double subduction model for the evolution of the North Tianshan Ocean. The continuous subduction created the Dananhu Arc in the north and the Central Tianshan Arc in the south. The Kangurtag belt in-between records the amalgamation of the Dananhu Arc and the Central Tianshan Arc.

Acknowledgments
We acknowledge Guoqing Han, Wei Lin, Zhonghua Tian, and Yichao Chen for their helpful discussions and Jiangjian Zhu for his assistance in the field. We thank Editor John Geissman, Associate Editor Jonathan Aitchison, and anonymous formal reviewers for their constructive comments that greatly improved the presentation of this paper. The study was financially supported by the National Key R&D Program of China (2017YFC0601206), the National Natural Science Foundation of China (41888101, 41730210, 41390441, 41230207, and 41202150), and the Key Research Program of Frontier Sciences, CAS (QYZDJ-SSW-SYS012). We also acknowledge institutional support from PROGRESS Q45 (Charles University). This is a contribution to IGCP 662. Data supplementing this paper are available in the supporting information Text S1, Figure S1, and Tables S1–S5.

References

Amato, J. M., Pavlis, T. L., Clift, P. D., Kochelek, E. J., Hecker, J. P., Worthman, C. M., & Day, E. M. (2013). Architecture of the Chugach accretionary complex as revealed by detrital zircon ages and lithologic variations: Evidence for Mesozoic subduction erosion in south-central Alaska. *Geological Society of America Bulletin*, *125*(11-12), 1891–1911. https://doi.org/10.1130/B30818.1

Bassett, K. N., & Orlowski, R. (2004). Pahau Terrane type locality: Fan delta in an accretionary prism trench-slope basin. *New Zealand Journal of Geology and Geophysics*, *47*(4), 603–623. https://doi.org/10.1080/00288306.2004.9515079

BGMRXUAR (1993). *Regional Geology of the Xinjiang Uygur Autonomous Region*, (p. 841). Beijing: Geological Publishing House.
Blichert-Toft, J., & Albarède, F. (1997). The Lu-Hf isotope geochemistry of chondrites and the evolution of the mantle-crust system. *Earth and Planetary Science Letters*, *148*(1-2), 243–258. https://doi.org/10.1016/S0012-821X(97)00040-X
Byrne, T., & Hibbard, J. (1987). Landward vergence in accretionary prisms: The role of the backstop and thermal history. *Geology*, *15*(12), 1163–1167. https://doi.org/10.1130/0091-7613(1987)15<1163:LVIAPT>2.0.CO;2
Boynton, W. V. (1984). Cosmochemistry of the Rare Earth Elements: Meteorite Studies. In P. Henderson (Ed.), *Developments in Geochemistry*, Neverlands: Elsevier (Vol. 2, pp. 63–114). https://doi.org/10.1016/B978-0-444-42148-7.50008-3
Cawood, P. A., Kröner, A., Collins, W. J., Kusky, T. M., Mooney, W. D., & Windley, B. F. (2009). Accretionary orogens through Earth history. In P. A. Cawood, & A. Kröner (Eds.), *Earth Accretionary Systems in Space and Time*, *Special Publications*, (Vol. 318, pp. 1–36). London: Geological Society. https://doi.org/10.1144/SP318.1
Charvet, J., Shu, L., & Laurent-Charvet, S. (2007). Paleozoic structural and geodynamic evolution of eastern Tianshan (NW China): Welding of the Tarim and Junggar plates. *Episodes*, *30*(3), 162–186.
Chen, X., Shu, L., & Ma, X. (2012). Geochemical features and tectonic significances of Weiya ophiolitic mélange and mafic granulite, Xinjiang. *Geological Journal of China Universities*, *18*(4), 661–675. (in Chinese with English abstract)
Chen, X., Shu, L., & Santosh, M. (2011). Late Paleozoic post-collisional magmatism in the Eastern Tianshan Belt, Northwest China: New insights from geochemistry, geochronology and petrology of bimodal volcanic rocks. *Lithos*, *127*(3-4), 581–598. https://doi.org/10.1016/j.lithos.2011.06.008
Danelian, T., & Robertson, A. H. F. (2001). Neotethyan evolution of eastern Greece (Pagondas Melange, Evia island) inferred from radiolarian biostratigraphy and the geochemistry of associated extrusive rocks. *Geological Magazine*, *138*(3), 345–363. https://doi.org/10.1017/S0016756801005337
DeCelles, P. G., Ducea, M. N., Kapp, P., & Zandt, G. (2009). Cyclicity in Cordilleran orogenic systems. *Nature Geoscience*, *2*(4), 251–257. https://doi.org/10.1038/ngeo469
Dickinson, W. R., & Gehrels, G. E. (2009). Use of U–Pb ages of detrital zircons to infer maximum depositional ages of strata: A test against a Colorado Plateau Mesozoic database. *Earth and Planetary Science Letters*, *288*(1-2), 115–125. https://doi.org/10.1016/j.epsl.2009.09.013
Dickinson, W. R., & Seely, D. (1979). Structure and stratigraphy of forearc regions. *AAPG Bulletin*, *63*(1), 2–31.
Douglass, J., Schilling, J. G., & Fontignie, D. (1999). Plume-ridge interactions of the Discovery and Shona mantle plumes with the southern Mid-Atlantic Ridge (40°-55°S). *Journal of Geophysical Research*, *104*(B2), 2941–2962. https://doi.org/10.1029/98JB02642
Du, L., Long, X., Yuan, C., Zhang, Y., Huang, Z., Sun, M., et al. (2018). Early Paleozoic dioritic and granitic plutons in the Eastern Tianshan Orogenic Belt, NW China: Constraints on the initiation of a magmatic arc in the southern Central Asian Orogenic Belt. *Journal of Asian Earth Sciences*, *153*, 139–153.
Festa, A., Pini, G. A., Dilek, Y., & Codegone, G. (2010). Mélanges and mélange-forming processes: A historical overview and new concepts. *International Geology Review*, *52*(10-12), 1040–1105. https://doi.org/10.1080/00206810903557704
Fitton, J. G. (2007). The OIB paradox. In R. F. Gillian, & M. J. Donna (Eds.), *Plates, Plumes, and Planetary Processes*, *Geological Society of America Bulletin*, (Vol. 430, pp. 387–412).
Frey, F. A., Walker, N., Stakes, D., Hart, S. R., & Nielsen, R. (1993). Geochemical characteristics of basaltic glasses from theamar and famous axial valleys, Mid-Atlantic Ridge (36–37 °N): Petrogenetic implications. *Earth and Planetary Science Letters*, *115*(1-4), 117–136. https://doi.org/10.1016/0012-821X(93)90217-W
Gehrels, G. E., Blakey, R., Karlstrom, K. E., Timmons, J. M., Dickinson, B., & Pecha, M. (2011). Detrital zircon U-Pb geochronology of Paleozoic strata in the Grand Canyon, Arizona. *Lithosphere*, *3*(3), 183–200. https://doi.org/10.1130/L121.1
Gibson, T., Myrow, P., Macdonald, F., Minjin, C., & Gehrels, G. (2013). Depositional history, tectonics, and detrital zircon geochronology of Ordovician and Devonian strata in southwestern Mongolia. *Geological Society of America Bulletin*, *125*(5-6), 877–893. https://doi.org/10.1130/B30746.1
Guo, Z., & Ma, R. (1990). A Study on The Later Paleozoic Kangguer inter-arc basin in Eastern Tianshan. *Journal of Nanjing University (Earth Science)*, *3*(1), 103–113. (in Chinese with English abstract)
Han, Y., & Zhao, G. (2018). Final amalgamation of the Tianshan and Junggar orogenic collage in the southwestern Central Asian Orogenic Belt: Constraints on the closure of the Paleo-Asian Ocean. *Earth-Science Reviews*, *186*, 129–152. https://doi.org/10.1016/j.earscirev.2017.09.012
Hashimoto, Y., & Kimura, G. (1999). Underplating process from melange formation to duplexing: Example from the Cretaceous Shimanto Belt, Kii Peninsula, southwest Japan. *Tectonics*, *18*(1), 92–107. https://doi.org/10.1029/1998TC900014
Hemond, C., Hofmann, A. W., Vlastelic, I., & Nauret, F. (2006). Origin of MORB enrichment and relative trace element compatibilities along the mid-Atlantic Ridge between 10 and 24 °N. *Geochemistry, Geophysics, Geosystems*, *7*, Q12010. https://doi.org/10.1029/2006GC001317
Hou, G., Tang, H., & Liu, C. (2006). Geochemical characteristics of the Late Paleozoic Volcanics in Jueluotage tectonic belt, eastern Tianshan and its implications. *Acta Petrologica Sinica*, *22*(5), 1167–1177. (in Chinese with English abstract)
Hsü, K. J., Guitang, P., & Sengör, A. (1995). Tectonic evolution of the Tibetan Plateau: A working hypothesis based on the archipelago model of orogenesis. *International Geology Review*, *37*(6), 473–508. https://doi.org/10.1080/00206819509465414
Huang, H., Wang, T., Qin, Q., Hou, J., Tong, Y., Guo, L., et al. (2015). Zircon Hf isotopic characteristics of granitoids from the Baluntai region, Central Tianshan: Implications for tectonic evolution and continental growth. *Acta Geologica Sinica*, *89*(12), 2286–2313. (in Chinese with English abstract)
Huang, W. (2014). Geochronology, geochemistry and formation of Carboniferous-Permian alkaline granite in Hami area, East Tianshan, MSc degree, China University of Geosciences, Beijing (in Chinese with English abstract).
Huang, Z. (2017). Precambrian crustal evolution of the Chinese Tianshan Belt, Ph. D thesis, 224 pp, Guangzhou Institute of Geochemisty, Chinese Academy of Sciences, Guangzhou, China (in Chinese with English abstract).
Ingersoll, R. V. (1988). Tectonics of sedimentary basins. *Geological Society of America Bulletin*, *100*(11), 1704–1719. https://doi.org/10.1130/0016-7606(1988)100<1704:TOSB>2.3.CO;2
Isozaki, Y., Aoki, K., Nakama, T., & Yanai, S. (2010). New insight into a subduction-related orogen: A reappraisal of the geotectonic framework and evolution of the Japanese Islands. *Gondwana Research*, *18*(1), 82–105. https://doi.org/10.1016/j.gr.2010.02.015
Isozaki, Y., Maruyama, S., & Furuoka, F. (1990). Accreted oceanic materials in Japan. *Tectonophysics*, *181*(1-4), 179–205. https://doi.org/10.1016/0040-1951(90)90016-2
Jackson, S. E., Pearson, N. J., Griffin, W. L., & Belousova, E. A. (2004). The application of laser ablation-inductively coupled plasma-mass spectrometry to in situ U–Pb zircon geochronology. *Chemical Geology*, *211*(1-2), 47–69. https://doi.org/10.1016/j.chemgeo.2004.06.017

Jahn, B.-M. (2004). The central Asian orogenic belt and growth of the continental crust in the Phanerozoic. In J. Malpas, C. J. N. Fletcher, J. R. Ali, & J. C. Aitchison (Eds.), *Aspects of the Tectonic Evolution of China*, *Special Publications*, (Vol. 226, pp. 73–100). London: Geological Society.

Jahn, B.-M., Wu, F. Y., & Chen, B. (2000). Granitoids of the Central Asian Orogenic Belt and continental growth in the Phanerozoic. *Transactions of the Royal Society of Edinburgh: Earth Sciences*, *91*(1-2), 181–193. https://doi.org/10.1017/S0263593300007367

Jiang, Y., Sun, M., Kröner, A., Tumurkhuu, D., Long, X., Zhao, G., et al. (2012). The high-grade Tseel Terrane in SW Mongolia: An Early Paleozoic arc system or a Precambrian sliver? *Lithos*, *142-143*, 95–115. https://doi.org/10.1016/j.lithos.2012.02.016

Jiang, Y., Sun, M., Zhao, G., Yuan, C., Xiao, W., Xia, X., et al. (2011). Precambrian detrital zircons in the Early Paleozoic Chinese Altai: Their provenance and implications for the crustal growth of central Asia. *Precambrian Research*, *189*(1-2), 140–154. https://doi.org/10.1016/j.precamres.2011.05.008

Kimura, G., & Ludden, J. (1995). Peeling oceanic crust in subduction zones. *Geology*, *23*(3), 217–220. https://doi.org/10.1130/0091-7613(1995)023<0217:POCISZ>2.3.CO;2

Kröner, A., Lehmann, J., Schulmann, K., Demoux, A., Lexa, O., Tomurhuu, D., et al. (2010). Lithostratigraphic and geochronological constraints on the evolution of the Central Asian Orogenic Belt in SW Mongolia: Early Paleozoic rifting followed by late Paleozoic accretion. *American Journal of Science*, *310*(7), 523–574. https://doi.org/10.2475/07.2010.01

Kröner, A., Windley, B., Badarch, G., Tomurtogoo, O., Hegner, E., Jahn, B., et al. (2007). Accretionary growth and crust formation in the Central Asian Orogenic Belt and comparison with the Arabian-Nubian shield. *Geological Society of America Memoirs*, *200*, 181–209. https://doi.org/10.1130/2007.1200(11)

Kusky, T. M., & Bradley, D. C. (1999). Kinematic analysis of mélange fabrics: Examples and applications from the McHugh Complex, Kenai Peninsula, Alaska. *Journal of Structural Geology*, *21*(12), 1773–1796. https://doi.org/10.1016/S0191-8141(99)00105-4

Kusky, T. M., Windley, B. F., Safonova, I., Wakita, K., Wakabayashi, J., Polat, A., & Santosh, M. (2013). Recognition of ocean plate stratigraphy in accretionary orogens through Earth history: A record of 3.8 billion years of sea floor spreading, subduction, and accretion. *Gondwana Research*, *24*(2), 501–547. https://doi.org/10.1016/j.gr.2013.01.004

Le Roux, P., Le Roex, A., Schilling, J.-G., Shimizu, N., Perkins, W., & Pearce, N. (2002). Mantle heterogeneity beneath the southern Mid-Atlantic Ridge: Trace element evidence for contamination of ambient asthenospheric mantle. *Earth and Planetary Science Letters*, *203*(1), 479–498. https://doi.org/10.1016/S0012-821X(02)00832-4

Leat, P., & Larter, R. (2003). Intra-oceanic subduction systems: Introduction. In P. Leat, & R. Larter (Eds.), *Intra-oceanic Subduction Systems: Tectonic and Magmatic Processes*, *Special Publications*, (Vol. 219, pp. 1–17). London: Geological Society. https://doi.org/10.1144/GSL.SP.2003.219.01.01

Leggett, J. K. (1985). Deep-sea pelagic sediments and palaeo-oceanography: A review of recent progress. In P. J. Brenchley, & P. Williams (Eds.), *Sedimentology Recent Developments and Applied Aspects*, *Special Publications*, (Vol. 18, pp. 95–121). London: Geological Society. https://doi.org/10.1144/GSL.SP.1985.018.01.06

Leggett, J. K., St. McKerrow, W., & Eales, M. H. (1979). The Southern Uplands of Scotland: A lower Paleozoic accretionary prism. *Journal of the Geological Society, London*, *136*(6), 755–770. https://doi.org/10.1144/gsjgs.136.6.0755

Lei, R., Wu, C., Gu, L., Zhang, Z., Chi, G., & Jiang, Y. (2011). Zircon U–Pb chronology and Hf isotope of the Xingxingxia granodiorite from the Central Tianshan zone (NW China): Implications for the tectonic evolution of the southern Altaids. *Gondwana Research*, *20*(2-3), 582–593. https://doi.org/10.1016/j.gr.2011.02.010

Lei, R., Wu, C., Qu, X., Gu, L., Chen, G., Uerna, A., et al. (2014). Geochronology, geochemistry and zircon Hf isotope compositions of the ore-bearing gneiss granite in the Tianhudong iron-molybdenum ore deposit in the Central Tianshan, West China: Implications for the Early Paleozoic tectonic evolution of Central Tianshan. *Journal of Jilin University (Earth Science Edition)*, *44*(5), 1540–1552. (in Chinese with English abstract)

Li, D.-F., Zhang, L., Chen, H.-Y., Hollings, P., Cao, M.-J., Fang, J., et al. (2016). Geochronology and geochemistry of the high Mg dioritic dikes in Eastern Tianshan, NW China: Geochemical features, petrogenesis and tectonic implications. *Journal of Asian Earth Sciences*, *115*, 442–454.

Li, J., Wang, K., Sun, G., Mo, S., Li, W., Yang, T., & Gao, L. (2006). Paleozoic active margin slices in the southern Turfan-Hami basin: Geological records of subduction of the Paleo-Asian Ocean plate in central Asian regions. *Acta Petrologica Sinica*, *22*(5), 1087–1102. (in Chinese with English abstract)

Li, J., Xiao, W., Wang, K., Sun, G., & Gao, L. (2003). Neoproterozoic-Paleozoic tectonostratigraphy, magmatic activities and tectonic evolution of eastern Xinjiang, NW China. In J. W. Mao, R. Goldfarb, R. Seltmann, D. H. Wang, W. J. Xiao, & C. J. Hart (Eds.), *Tectonic Evolution and Metallogeny of the Chinese Altay and Tianshan*, (pp. 31–74). London: CERAMS, Natural History Museum.

Li, P., Mu, L., Zhu, Z., Wang, K., Wang, Z., Qu, T., & Feng, J. (2017). Geochemistry and geochronology of granitoids intrusions from Baluntai area in central Mountains, and its tectonic significance. *Acta Geologica Sinica*, *91*(1), 80–93. (in Chinese with English abstract)

Li, Q., Liu, S., Song, B., Wang, Y., & Chen, Y. (2009). Late Mesoproterozoic to Paleozoic tectonothermal events in the Eastern Segment of the Central Tianshan Tectonic Zone of Northwestern China: Constraints from SHRIMP zircon geochronology. *Earth Science Frontiers*, *16*(2), 175–184.

Li, W.-Q., Ma, H., Wang, R., Wang, H., & Xia, B. (2008). SHRIMP dating and Nd-Sr isotopic Tracing of Kangguertage ophiolite in eastern Tianshan, Xinjiang. *Acta Petrologica Sinica*, *24*(4), 773–780. (in Chinese with English abstract)

Li, W.-Q., Xia, B., Wu, G., & Wang, H. (2005). Kangguertage ophiolite and tectonic significance, Shanshan, Xinjiang China. *Acta Petrologica Sinica*, *21*(6), 1617–1632. (in Chinese with English abstract)

Liu, S., Guo, Z. J., Zhang, Z. C., Li, Q. G., & Zheng, H. F. (2004). Nature of the Precambrian metamorphic blocks in the eastern segment of Central Tianshan: Constraint from geochronology and Nd isotopic geochemistry. *Science in China Series D-Earth Sciences*, *47*(12), 1085–1094. https://doi.org/10.1360/03yd0177

Long, X., & Huang, Z. (2017). Tectonic affinities of microcontinents in the Central Asian Orogenic Belt: A case study of the Chinese Tianshan orogenic belt. *Bulletin of Mineralogy, Petrology, and Geochemistry*, *36*(5), 771–785.

Long, X., Sun, M., Yuan, C., Xiao, W., Lin, S., Wu, F., et al. (2007). Detrital zircon age and Hf isotopic studies for metasedimentary rocks from the Chinese Altai: Implications for the early Paleozoic tectonic evolution of the central Asian orogenic belt. *Tectonics*, *26*, TC5015. https://doi.org/10.1029/2007TC002128

Long, X., Yuan, C., Sun, M., Xiao, W., Zhao, G., Wang, Y., et al. (2010). Detrital zircon ages and Hf isotopes of the early Paleozoic flysch sequence in the Chinese Altai, NW China: New constrains on depositional age, provenance and tectonic evolution. *Tectonophysics*, *480*(1-4), 213–231. https://doi.org/10.1016/j.tecto.2009.10.013

Ludwig, K. (2003). Mathematical-statistical treatment of data and errors for ^{230}Th/U geochronology. *Reviews in Mineralogy and Geochemistry*, *52*(1), 631–656. https://doi.org/10.2113/0520631

Luo, T., Liao, Q.-A., Zhang, X.-H., Chen, J.-P., Wang, G.-C., & Huang, X. (2016). Geochronology and geochemistry of Carboniferous metabasalts in eastern Tianshan, Central Asia: Evidence of a back-arc basin. *International Geology Review*, *58*(6), 756–772. https://doi.org/10.1080/00206814.2015.1114433

Ma, R., Ye, S., & Wang, C. (1993). *Tectonic framework and crustal evolution of Eastern Tianshan Mountains* (pp. 1–225). Nanjing, China: Publishing House of Nanjing University. (in Chinese with English abstract)

Ma, X., Shu, L., Jahn, B.-M., Zhu, W., & Faure, M. (2012). Precambrian tectonic evolution of Central Tianshan, NW China: Constraints from U-Pb dating and in situ Hf isotopic analysis of detrital zircons. *Precambrian Research*, *222-223*, 450–473.

Ma, X., Shu, L., Meert, J. G., & Li, J. (2014). The Paleozoic evolution of Central Tianshan: Geochemical and geochronological evidence. *Gondwana Research*, *25*(2), 797–819. https://doi.org/10.1016/j.gr.2013.05.015

Ma, X., Shu, L., Santosh, M., & Li, J. (2012). Detrital zircon U-Pb geochronology and Hf isotope data from Central Tianshan suggesting a link with the Tarim block: Implications for Proterozoic supercontinent history. *Precambrian Research*, *206-207*, 1–16. https://doi.org/10.1016/j.precamres.2012.02.015

Ma, X., Shu, L., Santosh, M., & Li, J. (2013). Petrogenesis and tectonic significance of an early Paleozoic mafic-intermediate suite of rocks from the Central Tianshan, northwest China. *International Geology Review*, *55*(5), 548–573. https://doi.org/10.1080/00206814.2012.727575

Mao, Q., Wang, J., Xiao, W., Fang, T., Wang, N., & Yu, M. (2014). The discovery of low-Carboniferous arc volcanic rocks and its tectonic significance at the Kalatage area in the Central Tianshan, Eastern Tianshan Mountains, Xinjiang, NW China. *Acta Geologica Sinica*, *88*(10), 1790–1799. (in Chinese with English abstract)

Mao, Q., Wang, J., Xiao, W., Windley, B. F., Schulmann, K., Yu, M., et al. (2018). Mineralization of an intra-oceanic arc in an accretionary orogen: Insights from the Early Silurian Honghai volcanogenic massive sulfide Cu-Zn deposit and associated adakites of the Eastern Tianshan (NW China). *Geological Society of America Bulletin*, *131*(5-6), 803–830. https://doi.org/10.1130/B31986.1

Mao, Q., Xiao, W., Fang, T., Windley, B. F., Sun, M., Ao, S., et al. (2014). Geochronology, geochemistry and petrogenesis of Early Permian alkaline magmatism in the Eastern Tianshan: Implications for tectonics of the Southern Altaids. *Lithos*, *190-191*, 37–51. https://doi.org/10.1016/j.lithos.2013.11.011

Maruyama, S., Kawai, T., & Windley, B. (2010). Ocean plate stratigraphy and its imbrication in an accretionary orogen: The Mona Complex, Anglesey–Lleyn, Wales, UK. In T. M. Kusky, M.-G. Zhai, & W. Xiao (Eds.), *The Evolving Continents: Understanding Processes of Continental Growth*, *Special Publications*, (Vol. 338, pp. 55–75). London: Geological Society. https://doi.org/10.1144/SP338.4

Matsuda, T., & Isozaki, Y. (1991). Well-documented travel history of Mesozoic pelagic chert in Japan: From remote ocean to subduction zone. *Tectonics*, *10*(2), 475–499. https://doi.org/10.1029/90TC02134

McCall, G., & Kidd, R. (1982). The Makran, southeastern Iran: The anatomy of a convergent plate margin active from Cretaceous to Present. In J. K. Leggett (Ed.), *Trench-Forearc Geology: Sedimentation and Tectonics on Modern and Ancient Active Plate Margins*, *Special Publications*, (Vol. 10, pp. 387–397). London: Geological Society. https://doi.org/10.1144/GSL.SP.1982.010.01.26

McKerrow, W. S., Leggett, J., & Eales, M. (1977). Imbricate thrust model of the Southern Uplands of Scotland. *Nature*, *267*(5608), 237–239. https://doi.org/10.1038/267237a0

Meschede, M. (1986). A method of discriminating between different types of mid-ocean ridge basalts and continental tholeiites with the Nb-Zr-Y diagram. *Chemical Geology*, *56*(3-4), 207–218. https://doi.org/10.1016/0009-2541(86)90004-5

Mišković, A., & Schaltegger, U. (2009). Crustal growth along a non-collisional cratonic margin: A Lu–Hf isotopic survey of the Eastern Cordilleran granitoids of Peru. *Earth and Planetary Science Letters*, *279*(3-4), 303–315. https://doi.org/10.1016/j.epsl.2009.01.002

Mohammadi, A., Burg, J.-P., Winkler, W., Ruh, J., & von Quadt, A. (2016). Detrital zircon and provenance analysis of Late Cretaceous–Miocene onshore Iranian Makran strata: Implications for the tectonic setting. *Geological Society of America Bulletin*, *128*(9-10), 1481–1499. https://doi.org/10.1130/B31361.1

Moore, G., Billman, H., Hehanussa, P., & Karig, D. (1980). Sedimentology and paleobathymetry of Neogene trench-slope deposits, Nias Island, Indonesia. *Journal of Geology*, *88*(2), 161–180. https://doi.org/10.1086/628489

Moore, G. F., & Karig, D. (1980). Structural geology of Nias Island, Indonesia; implications for subduction zone tectonics. *American Journal of Science*, *280*(3), 193–223. https://doi.org/10.2475/ajs.280.3.193

Moore, J. C., & Silver, E. A. (1987). Continental margin tectonics: Submarine accretionary prisms. *Reviews of Geophysics*, *25*(6), 1305–1312. https://doi.org/10.1029/RG025i006p01305

Murton, B. J., Tindle, A. G., Milton, J. A., & Sauter, D. (2005). Heterogeneity in southern Central Indian Ridge MORB: Implications for ridge–hot spot interaction. *Geochemistry, Geophysics, Geosystems*, *6*, Q03E20. https://doi.org/10.1029/2004GC000798

Nijat, A., Muhtar, Z., & Wu, Z. (2015). Zircon U-Pb isotopic chronology and Hf isotopes of diorites from Kawabulak Complex, Central Tianshan. *Journal of Jilin University*, *45*(6), 1702–1712. (in Chinese with English abstract)

Onishi, C. T., & Kimura, G. (1995). Change in fabric of mélange in the Shimanto Belt, Japan: Change in relative convergence? *Tectonics*, *14*(6), 1273–1289. https://doi.org/10.1029/95TC01929

Pearce, J. A., & Cann, J. (1973). Tectonic setting of basic volcanic rocks determined using trace element analyses. *Earth and Planetary Science Letters*, *19*(2), 290–300. https://doi.org/10.1016/0012-821X(73)90129-5

Perk, N. W., Coogan, L. A., Karson, J. A., Klein, E. M., & Hanna, H. D. (2007). Petrology and geochemistry of primitive lower oceanic crust from Pito Deep: Implications for the accretion of the lower crust at the Southern East Pacific Rise. *Contributions to Mineralogy and Petrology*, *154*(5), 575–590. https://doi.org/10.1007/s00410-007-0210-z

Regelous, M., Hofmann, A., Abouchami, W., & Galer, S. (2003). Geochemistry of lavas from the Emperor Seamounts, and the geochemical evolution of Hawaiian magmatism from 85 to 42 Ma. *Journal of Petrology*, *44*(1), 113–140. https://doi.org/10.1093/petrology/44.1.113

Rojas-Agramonte, Y., Kröner, A., Demoux, A., Xia, X., Wang, W., Donskaya, T., et al. (2011). Detrital and xenocrystic zircon ages from Neoproterozoic to Palaeozoic arc terranes of Mongolia: Significance for the origin of crustal fragments in the Central Asian Orogenic Belt. *Gondwana Research*, *19*(3), 751–763. https://doi.org/10.1016/j.gr.2010.10.004

Safonova, I., Maruyama, S., Kojima, S., Komiya, T., Krivonogov, S., & Koshida, K. (2016). Recognizing OIB and MORB in accretionary complexes: A new approach based on ocean plate stratigraphy, petrology and geochemistry. *Gondwana Research*, *33*, 92–114. https://doi.org/10.1016/j.gr.2015.06.013

Sawaki, Y., Shibuya, T., Kawai, T., Komiya, T., Omori, S., Iizuka, T., et al. (2010). Imbricated ocean-plate stratigraphy and U-Pb zircon ages from tuff beds in cherts in the Ballantrae complex, SW Scotland. *Geological Society of America Bulletin*, *122*(3-4), 454–464. https://doi.org/10.1130/B26329.1

Scherer, E., Münker, C., & Mezger, K. (2001). Calibration of the lutetium-hafnium clock. *Science*, *293*(5530), 683–687. https://doi.org/10.1126/science.1061372

Schilling, J., Zajac, M., Evans, R., Johnston, T., White, W., Devine, J., & Kingsley, R. (1983). Petrologic and geochemical variations along the Mid-Atlantic Ridge from 29 degrees N to 73 degrees N. *American Journal of Science*, *283*(6), 510–586. https://doi.org/10.2475/ajs.283.6.510

Sengör, A., Natal'In, B., & Burtman, V. (1993). Evolution of the Altaid tectonic collage and Palaeozoic crustal growth in Eurasia. *Nature*, *364*(6435), 299–307. https://doi.org/10.1038/364299a0

Shi, Y., Jian, P., Kröner, A., Jahn, B.-M., Liu, D., Zhang, W., & Ma, H. (2014). Zircon ages and Hf isotopic compositions of plutonic rocks from the Central Tianshan (Xinjiang, northwest China) and their significance for early to mid-Palaeozoic crustal evolution. *International Geology Review*, *56*(11), 1413–1434. https://doi.org/10.1080/00206814.2014.942807

Shu, L., Charvet, J., Lu, H. F., & Laurent, S. C. (2002). Paleozoic accretion-collision events and kinematics of ductile deformation in the eastern part of the Southern-Central Tianshan belt, China. *Acta Geologica Sinica (English Edition)*, *76*(3), 308–323.

Shu, L., Yu, J. H., Charvet, J., Laurent-Charvet, S., Sang, H. Q., & Zhang, R. G. (2004). Geological, geochronological and geochemical features of granulites in the Eastern Tianshan, NW China. *Journal of Asian Earth Sciences*, *24*(1), 25–41. https://doi.org/10.1016/j.jseaes.2003.07.002

Stern, R. J. (2010). The anatomy and ontogeny of modern intra-oceanic arc systems. In T. M. Kusky, M.-G. Zhai, & W. Xiao (Eds.), *The Evolving Continents: Understanding Processes of Continental Growth*, *Special Publications*, (Vol. 338, pp. 7–34). London: Geological Society. https://doi.org/10.1144/SP338.2

Su, C., Jiang, C., Xia, M., Zhang, L., Ji, H., Guo, F., & Liu, X. (2008). Zircon SHRIMP U-Pb dating from granite of the metamorphic core complex system in Jueluotage tectonic belt and its geological significance. *Acta Petrologica Sinica*, *24*(12), 2789–2799. (in Chinese with English abstract)

Sun, S.-S., & McDonough, W. (1989). Chemical and isotopic systematics of oceanic basalts: Implications for mantle composition and processes. In A. D. Saunders, & M. J. Norry (Eds.), *Magmatism in the Ocean Basins*, *Special Publications*, (Vol. 42, pp. 313–345). London: Geological Society. https://doi.org/10.1144/GSL.SP.1989.042.01.19

Sun, S.-S., Nesbitt, R. W., & Sharaskin, A. Y. (1979). Geochemical characteristics of mid-ocean ridge basalts. *Earth and Planetary Science Letters*, *44*(1), 119–138. https://doi.org/10.1016/0012-821X(79)90013-X

Sun, Y., Wang, J., Li, Y., Wang, Y., Yu, M., Long, L., et al. (2017). Recognition of Late Ordovician Yudai porphyry Cu (Au, Mo) mineralization in the Kalatag district, Eastern Tianshan terrane, NW China: Constraints from geology, geochronology, and petrology. *Ore Geology Reviews*, *100*, 220–236.

Taira, A. (2001). Tectonic evolution of the Japanese island arc system. *Annual Review of Earth and Planetary Sciences*, *29*(1), 109–134. https://doi.org/10.1146/annurev.earth.29.1.109

Taira, A., Okada, H., Whitaker, J. H., & Smith, A. J. (1982). The Shimanto Belt of Japan: cretaceous-lower Miocene active-margin sedimentation. In J. K. Leggett (Ed.), *Trench-Forearc Geology: Sedimentation and Tectonics on Modern and Ancient Active Plate Margins*, *Special Publications*, (Vol. 10, pp. 5–26). London: Geological Society. https://doi.org/10.1144/GSL.SP.1982.010.01.01

Tang, Z., Cai, Z., Wang, Z., & Chen, F. (2011). Deformational characteristics of ductile shear zones in northern and southern margins of eastern central Tianshan. *Geology in China*, *38*(4), 970–979. (in Chinese with English abstract)

Underwood, M. B., & Bachman, S. B. (1986). Sandstone petrofacies of the Yager complex and the Franciscan Coastal belt, Paleogene of northern California. *Geological Society of America Bulletin*, *97*(7), 809–817. https://doi.org/10.1130/0016-7606(1986)97<809:SPOTYC>2.0.CO;2

Underwood, M. B., & Moore, G. F. (1998). Trenches and Trench slope basins. In C. Busby, & R. Ingersoll (Eds.), *Tectonics of Sedimentary Basins*, (pp. 179–219). New Jersey, USA: Wiley-Blackwell.

Wakabayashi, J., & Dilek, Y. (2011). Mélanges of the Franciscan Complex, California: Diverse structural settings, evidence for sedimentary mixing, and their connection to subduction processes. In J. Wakabayashi (Ed.), *Mélanges: processes of formation and societal significance*, *Geological Society of America Special Paper*, (Vol. 480, pp. 117–141). https://doi.org/10.1130/2011.2480(05)

Wakita, K. (2012). Mappable features of mélanges derived from Ocean Plate Stratigraphy in the Jurassic accretionary complexes of Mino and Chichibu terranes in Southwest Japan. *Tectonophysics*, *568–569*, 74–85.

Wakita, K. (2015). OPS mélange: a new term for mélanges of convergent margins of the world. *International Geology Review*, *57*(5-8), 529–539. https://doi.org/10.1080/00206814.2014.949312

Wakita, K., & Metcalfe, I. (2005). Ocean plate stratigraphy in East and Southeast Asia. *Journal of Asian Earth Sciences*, *24*(6), 679–702. https://doi.org/10.1016/j.jseaes.2004.04.004

Wang, H. (2007), *Geological Map of Chinese Tianshan and Adjacent Areas* (scale 1:1,000,000), Xi'an, China: Xi'an Center of China Geological Survey.

Wang, Y., Long, X., Wilde, S. A., Xu, H., Sun, M., Xiao, W., et al. (2014). Provenance of Early Paleozoic metasediments in the central Chinese Altai: Implications for tectonic affinity of the Altai-Mongolia terrane in the Central Asian Orogenic Belt. *Lithos*, *210-211*, 57–68. https://doi.org/10.1016/j.lithos.2014.09.026

Wang, Y.-F., Chen, H., Han, J., Chen, S., Huang, B., Li, C., et al. (2018). Paleozoic tectonic evolution of the Dananhu-Tousuquan island arc belt, Eastern Tianshan: Constraints from the magmatism of the Yuhai porphyry Cu deposit, Xinjiang, NW China. *Journal of Asian Earth Sciences*, *153*, 282–306.

Wang, Y.-H., Xue, C., Liu, J., Wang, J., Yang, J., Zhang, F., et al. (2015). Early Carboniferous adakitic rocks in the area of the Tuwu deposit, eastern Tianshan, NW China: Slab melting and implications for porphyry copper mineralization. *Journal of Asian Earth Sciences*, *103*, 332–349.

Wang, Y.-H., Xue, C., Wang, J., Peng, R., Yang, J., Zhang, F., et al. (2015). Petrogenesis of magmatism in the Yandong region of Eastern Tianshan, Xinjiang: Geochemical, geochronological, and Hf isotope constraints. *International Geology Review*, *57*(9-10), 1130–1151. https://doi.org/10.1080/00206814.2014.900653

Wang, Y.-H., & Zhang, F. (2016). Petrogenesis of early Silurian intrusions in the Sanchakou area of Eastern Tianshan, Northwest China, and tectonic implications: Geochronological, geochemical, and Hf isotopic evidence. *International Geology Review*, *58*(10), 1294–1310. https://doi.org/10.1080/00206814.2016.1152516

Wang, Y.-H., Zhang, F., & Liu, J. (2016). The genesis of the ores and intrusions at the Yuhai Cu-Mo deposit in eastern Tianshan, NW China: Constraints from geology, geochronology, geochemistry, and Hf isotope systematics. *Ore Geology Reviews*, *77*, 312–331.

Wang, Y.-H., Zhang, F., Liu, J., & Que, C. (2016). Carboniferous magmatism and mineralization in the area of the Fuxing Cu deposit, Eastern Tianshan, China: Evidence from zircon U–Pb ages, petrogeochemistry, and Sr–Nd–Hf–O isotopic compositions. *Gondwana Research*, *34*, 109–128.

Weaver, B. L. (1991). The origin of ocean island basalt end-member compositions: Trace element and isotopic constraints. *Earth and Planetary Science Letters*, *104*(2-4), 381–397. https://doi.org/10.1016/0012-821X(91)90217-6

Westbrook, G. K., Ladd, J. W., Buhl, P., Bangs, N., & Tiley, G. J. (1988). Cross section of an accretionary wedge: Barbados Ridge complex. *Geology*, *16*(7), 631–635. https://doi.org/10.1130/0091-7613(1988)016<0631:CSOAAW>2.3.CO;2

White, W. M. (2010). Oceanic island basalts and mantle plumes: The geochemical perspective. *Annual Review of Earth and Planetary Sciences*, *38*(1), 133–160. https://doi.org/10.1146/annurev-earth-040809-152450

Wilson, B. M. (2007). Island Arcs. In B. M. Wilson (Ed.), *Igneous Petrogenesis a Global Tectonic Approach* (pp. 153–190). Netherlands: Springer Science & Business Media.

Winchester, J., & Floyd, P. (1977). Geochemical discrimination of different magma series and their differentiation products using immobile elements. *Chemical Geology*, *20*, 325–343. https://doi.org/10.1016/0009-2541(77)90057-2

Windley, B. F., Alexeiev, D., Xiao, W., Kröner, A., & Badarch, G. (2007). Tectonic models for accretion of the Central Asian Orogenic Belt. *Journal of the Geological Society*, *164*(1), 31–47. https://doi.org/10.1144/0016-76492006-022

Wood, D. A. (1980). The application of a ThHfTa diagram to problems of tectonomagmatic classification and to establishing the nature of crustal contamination of basaltic lavas of the British Tertiary Volcanic Province. *Earth and Planetary Science Letters*, *50*(1), 11–30. https://doi.org/10.1016/0012-821X(80)90116-8

Wu, F., Ji, W., Liu, C., & Chung, S. (2010). Detrital zircon U–Pb and Hf isotopic data from the Xigaze fore-arc basin: Constraints on Transhimalayan magmatic evolution in southern Tibet. *Chemical Geology*, *271*(1–2), 13–25. https://doi.org/10.1016/j.chemgeo.2009.12.007

Wu, F., Yang, Y., Xie, L., Yang, J., & Xu, P. (2006). Hf isotopic compositions of the standard zircons and baddeleyites used in U–Pb geochronology. *Chemical Geology*, *234*(1-2), 105–126. https://doi.org/10.1016/j.chemgeo.2006.05.003

Xiao, B., Chen, H., Hollings, P., Han, J., Wang, Y., Yang, J., & Cai, K. (2017). Magmatic evolution of the Tuwu–Yandong porphyry Cu belt, NW China: Constraints from geochronology, geochemistry and Sr–Nd–Hf isotopes. *Gondwana Research*, *43*, 74–91.

Xiao, W., Windley, B., Allen, M. B., & Han, C. M. (2013). Paleozoic multiple accretionary and collisional tectonics of the Chinese Tianshan orogenic collage. *Gondwana Research*, *23*(4), 1316–1341. https://doi.org/10.1016/j.gr.2012.01.012

Xiao, W., Windley, B., Huang, B., Han, C., Yuan, C., Chen, H., et al. (2009). End-Permian to mid-Triassic termination of the accretionary processes of the southern Altaids: Implications for the geodynamic evolution, Phanerozoic continental growth, and metallogeny of Central Asia. *International Journal of Earth Sciences*, *98*(6), 1189–1217. https://doi.org/10.1007/s00531-008-0407-z

Xiao, W., Windley, B., Sun, S., Li, J., Huang, B., Han, C., et al. (2015). A tale of amalgamation of three Permo-Triassic collage systems in Central Asia: Oroclines, sutures, and terminal accretion. *Annual Review of Earth and Planetary Sciences*, *43*(1), 477–507. https://doi.org/10.1146/annurev-earth-060614-105254

Xiao, W., Windley, B. F., Hao, J., & Zhai, M. (2003). Accretion leading to collision and the Permian Solonker suture, Inner Mongolia, China: Termination of the central Asian orogenic belt. *Tectonics*, *22*(6), 1069. https://doi.org/10.1029/2002TC001484

Xiao, W., Zhang, L. C., Qin, K. Z., Sun, S., & Li, J. L. (2004). Paleozoic accretionary and collisional tectonics of the Eastern Tianshan (China): Implications for the continental growth of Central Asia. *American Journal of Science*, *304*(4), 370–395. https://doi.org/10.2475/ajs.304.4.370

Xu, X., Xia, L., Ma, Z., Wang, Y., Xia, Z., Li, X., & Wang, L. (2006). SHRIMP Zircon U-Pb geochronology of the plagiogranites from Bayingou ophiolite in North Tianshan Mountains and the Petrogenesis of the Ophiolite. *Acta Petrologica Sinica*, *22*(1), 83–94. (in Chinese with English abstract)

Xu, X.-Y., Wang, H., Ma, G.-L., Li, P., Chen, J., & Li, T. (2010). Geochronology and Hf isotope characteristics of the Paleozoic granite in Nalati area, West Tianshan Mountains. *Acta Petrologica et Mineralogica*, *29*(6), 691–706. (in Chinese with English abstract)

Yang, M., Wang, J., Wang, J., & Dang, F. (2012). Studies on geochemistry, zircon U-Pb geochronology and Hf isotopes of granite in Wangfeng area at the northern margin of Middle Tianshan, Xinjiang. *Acta Petrologica Sinica*, *28*(7), 2121–2131. (in Chinese with English abstract)

Yin, J., Chen, W., Xiao, W., Yuan, C., Zhang, B., Cai, K., & Long, X. (2017). Geochronology, petrogenesis, and tectonic significance of the latest Devonian–early Carboniferous I-type granites in the Central Tianshan, NW China. *Gondwana Research*, *47*, 188–199. https://doi.org/10.1016/j.gr.2016.02.012

Zhang, F., Wang, Y., & Liu, J. (2016). Petrogenesis of Late Carboniferous granitoids in the Chihu area of Eastern Tianshan, Northwest China, and tectonic implications: Geochronological, geochemical, and zircon Hf–O isotopic constraints. *International Geology Review*, *58*(8), 949–966. https://doi.org/10.1080/00206814.2015.1136800

Zhang, L., Xiao, W., Qin, K., & Zhang, Q. (2006). The adakite connection of the Tuwu-Yandong copper porphyry belt, eastern Tianshan, NW China: Trace element and Sr-Nd-Pb isotope geochemistry. *Mineralium Deposita*, *41*(2), 188–200. https://doi.org/10.1007/s00126-006-0058-6

Zhang, X.-R., Zhao, G., Eizenhofer, P. R., Sun, M., Han, Y., Hou, W., et al. (2015). Latest Carboniferous closure of the Junggar Ocean constrained by geochemical and zircon U-Pb-Hf isotopic data of granitic gneisses from the Central Tianshan block, NW China. *Lithos*, *238*, 26–36. https://doi.org/10.1016/j.lithos.2015.09.012

Zhang, X.-R., Zhao, G., Eizenhöfer, P. R., Sun, M., Han, Y., Hou, W., et al. (2016a). Tectonic transition from Late Carboniferous subduction to Early Permian post-collisional extension in the Eastern Tianshan, NW China: Insights from geochronology and geochemistry of mafic–intermediate intrusions. *Lithos*, *256-257*, 269–281.

Zhang, X.-R., Zhao, G., Eizenhöfer, P. R., Sun, M., Han, Y., Hou, W., et al. (2016b). Late Ordovician adakitic rocks in the Central Tianshan block, NW China: Partial melting of lower continental arc crust during back-arc basin opening. *Geological Society of America Bulletin*, *128*(9-10), 1367–1382. https://doi.org/10.1130/B31452.1

Zhang, X.-R., Zhao, G., Sun, M., Eizenhofer, P. R., Han, Y., Hou, W., et al. (2016). Tectonic evolution from subduction to arc-continent collision of the Junggar ocean: Constraints from U-Pb dating and Hf isotopes of detrital zircons from the North Tianshan belt, NW China. *Geological Society of America Bulletin*, *128*(3-4), 644–660. https://doi.org/10.1130/B31230.1

Zhang, Y.-Y., Sun, M., Yuan, C., Long, X., Jiang, Y., Li, P., et al. (2018). Alternating trench advance and retreat: Insights from Paleozoic magmatism in the eastern Tianshan, Central Asian Orogenic Belt. *Tectonics*, *7*, 2142–2164. https://doi.org/10.1029/2018TC005051

Zhou, T., Yuan, F., Zhang, D., Fan, Y., Liu, S., Peng, M., & Zhang, J. (2010). Geochronology, tectonic setting and mineralization of granitoids in Jueluotage area, eastern Tianshan, Xinjiang. *Acta Petrologica Sinica*, *26*(2), 478–502. (in Chinese with English abstract)

Zhu, M., Wu, G., Xie, H., Liu, J., & Zhang, L. (2011). Geochronology and geochemistry of the Kekesai intrusion in western Tianshan, NW China and its geological implications. *Acta Petrologica Sinica*, *27*(10), 3041–3054. (in Chinese with English abstract)

Zhu, W., Shu, L., Ma, R., & Sun, Y. (2004). Comment on "Characteristics and dynamic origin of the large-scale Jiaoluotage ductile compressional zone in the eastern Tianshan Mountains, China" by XW Xu, TL Ma, LQ Sun and XP Cai: (Journal of Structural Geology 25 (2003) 1901–1916) doi of original article: 10.1016/S0191-8141 (03) 000178. *Journal of Structural Geology*, *26*(12), 2331–2335.